Design Guidelines for Optical Camera Communication Systems: A Tutorial

Anqi Liu, Wenxiao Shi, *Member, IEEE*, Majid Safari, Wei Liu, and Jingtai Cao

***Abstract*—The rapid development of the Internet of Things (IoT) has put great challenges on the next generation's communication technologies. Optical Camera Communication (OCC), with its advantages of the green principle, less electromagnetic interference, and harmonious integrations, can serve as a complementary, and sometimes viable alternative technology to mainstream Radio Frequency (RF)-based one. Designing efficient OCC platforms crucially involves accurate modeling of the OCC system and evaluating the efficiency of OCC-based techniques, which then stimulates related practical applications. This paper aims to provide a systematic perspective to understand OCC and to present design guidelines for OCC systems from theory to practice. First, the main parameters and analytical models for OCC basic components are presented to provide guidance on hardware parameter selection and system simulations. Next, typical implementation procedures and common performance evaluation criteria for an overall OCC system are provided. Then, detailed goal-oriented OCC enhancement solutions are summarized aiming to provide systematic guidelines for system performance enhancement. Finally, OCC designed examples are presented based on the results of our OCC experimental platform and some future research directions are discussed.**

***Index Terms*—Analytical models, design guidelines, image processing, Internet of Things (IoT), optical camera communication (OCC), performance evaluation and enhancement.**

I. Introduction

THE rapid increase in miscellaneous digital services and the widespread application of the Internet of Things (IoT) have put more strict requirements on the supported bandwidth, reliability, green, and safe properties for the next generation's communication technologies [1]. Disadvantages of the frequency spectrum scarcity, electromagnetic interference, and the vulnerabilities to eavesdropping that existed in the mainstream Radio Frequency (RF)-based communication systems have put great obstacles to satisfying the above-mentioned demands [2]. A complementary, and sometimes viable alternative technology is therefore of great significance. Optical Camera Communication (OCC), with its advantages of unlicensed spectrum with no radio frequency interference and joint sensing and communication capability can be considered as a promising complementary solution [3] for easing the bandwidth usage pressure on RF systems in a harmonious manner. Recent developments in semiconductor manufacturing have witnessed the proliferating use of Light-Emitting Diode (LED) and camera at a much lower cost. The pervasive but cost-efficient utilization of the transceivers then further stimulates the research interests and wide applications of OCC in IoT-based financial, technical, medical, and social fields [2], [3], [4].

Manuscript received 27 March 2024; revised 2 July 2024; accepted 3 July 2024. Date of publication 9 July 2024; date of current version 31 July 2024. This work was supported in part by the National Natural Science Foundation of China under Grant 61601195, in part by the Science and Technology Development Plan of Jilin Province under Grant 20200401122GX, in part by Jilin Provincial Scientific and Technological Development Program under Grant 20210203042SF, and in part by the China Scholarship Council (CSC) under Grant 202206170080. *(Corresponding author: Wenxiao Shi.)*

Anqi Liu, Wenxiao Shi, and Wei Liu are with the College of Communication Engineering, Jilin University, Changchun 130012, China (e-mail: liuaq21@mails.jlu.edu.cn; swx@jlu.edu.cn; jdlw@jlu.edu.cn).

Majid Safari is with the School of Engineering, Institute for Imaging, Data, and Communications, University of Edinburgh, EH9 3FD Edinburgh, U.K. (e-mail: majid.safari@ed.ac.uk).

Jingtai Cao is with the College of Communication Engineering, Jilin University, Changchun 130012, China, and also with the Changchun Institute of Optics, Fine Mechanics and Physics, Chinese Academy of Sciences, Changchun 130033, China (e-mail: jingtai1985@163.com).

Digital Object Identifier 10.1109/JPHOT.2024.3424885

A. Literature Review

The current literature on OCC includes some tutorial papers with contents which can be roughly classified into four categories including technology overview [5], [6], [7], [8], [9], [10], standard analysis [11], [12], [13], [14], [15], OCC-based application scenarios [2], [4], [16], [17], [18], and key OCC techniques investigations [19], [20], [21]. The first category of papers concentrates on operation principles [5], [6], basic components [7], [8], [9], practical challenges [8], and future research perspectives [10]. The standard-related papers [11], [12], [13] provide insights into the motivation and revision details of the IEEE 802.15.7r1 with frame format design of the OCC Medium Access Control (MAC) layer. Developments for IEEE 802.15.7a (TG7a) standard are described and introduced in [12], [13]. The application-specific tutorials consider OCC for IoT [2], the 5th Generation (5G) network [4], the smartphone-based system [16], the eHealth field [17], and the vehicular communication network [18] to demonstrate their compatibility and adaptability. OCC key techniques, such as undersampled-based modulation [19], OCC Deep Learning (DL)-aided methods [20], and security issues [21] have been investigated systematically in the key techniques-based papers.

Although some OCC design-related contributions have been made in these papers, there still remains a gap for a tutorial that provides a comprehensive OCC design guideline from theory to practice. First, a systematic review of OCC system key parameters characteristics and analytical models for OCC transceivers and optical channels is missing in the literature. The

study of key parameters is beneficial in OCC hardware design for experimental platforms, and this along with OCC system models can provide theoretical support for simulating OCC systems. Second, technical design approaches for experimental OCC platforms are not sufficiently provided and detailed procedures for accurate simulations of an OCC system are seldom discussed in the existing OCC tutorial papers. Finally, performance enhancement solutions for the OCC system designs based on various communication requirements are not comprehensively reviewed.

B. Our Contributions

Based on the above-analyzed limitations, the contributions of this paper can be summarized as follows.

- Main parameters of the OCC transceiver and its channel are systematically characterized to provide hardware parameter selection guidelines for experimental OCC systems design. Analytical models of the LED-based transmitter, camera, and optical channels are summarized to support the simulation of OCC system design.
- Implementation procedures for both the experimental and simulated OCC systems are introduced to provide guidance for an overall system design. Common performance criteria are also summarized to help evaluate the system's performance.
- Detailed performance enhancement approaches to achieve various OCC requirements including communication speed improvement, distance extension, quality increase, and reliability enhancement are comprehensively presented.
- Detailed design examples of both experimental and simulated OCC setups are presented. Both indoor and outdoor application scenarios are discussed for experimental setups elaborating on selected transceiver types, applied algorithms, challenges, achieved communication performance, and future design suggestions. Simulation methods, synthetic OCC images, and theoretical performance analysis are also illustrated based on our simulated OCC systems.

C. Scope of This Paper

This paper is divided into the sections listed below. OCC preliminaries which include its general features, related standards, and main system categories are provided in Section II serving as a technology background. Common components, their main parameters, and analytical models are summarized in Section III. Section IV introduces implementation and evaluation criteria for both the experimental and simulated OCC systems. Detailed OCC performance enhancement approaches for various communication requirements are demonstrated in Section V. Typical OCC design examples based on both the simulated and experimental setup platforms are manifested in Section VI. Design challenges and future research directions are presented in Section VII. Concluding remarks are summarized in Section VIII.

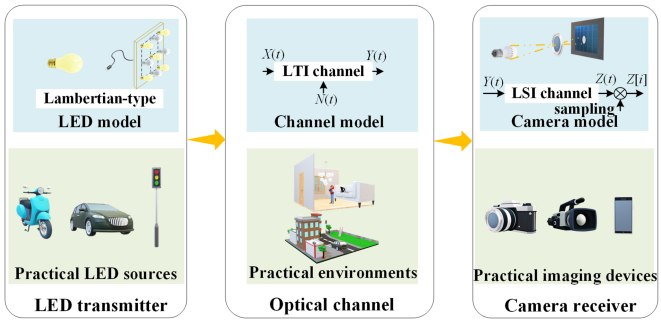

Fig. 1. OCC basic structure, where LED-based transmitter, optical channel, and camera receiver are three basic components.

II. OCC Preliminaries

OCC, also known as Camera Communication (CamCom), light-to-camera communication, and Image Sensor Communication (ISC), is one of the Optical Wireless Communication (OWC) technologies. It helps to realize wireless connectivity based on the three frequency bands of Infrared (IR: 3–300 THz), Visible Light (VL: 380–790 THz), and Ultraviolet (UV: 790–3000 THz) [4]. The history of OCC could be dated back to 2001 when the camera receiver was first presented in the optical communication field [5]. It was then first included in the revised IEEE 802.15.7r1 standard, which originated from the IEEE 802.15.7-2011 standard for Visible Light Communication (VLC). A task group called TG7m was founded in 2014 to not only develop the OCC technical requirements but also revise the standard known as IEEE 802.15.7 m which is mainly targeted for short-range communications [18]. Specifications were finally approved in 2018 with the title updated to IEEE 802.15.7:2018, where the defined Physical layers (PHY) have increased from three in 2011 to six. Task Group 7a has recently been initiated to further produce an amendment to IEEE 802.15.7-2018 which focuses more on improving the data rate, extending communication distances, and supporting system mobility [12], [14], [15]. A new PHY specification mode and wide-range multi-carrier modulation techniques have been accepted for OCC applications. Orthogonal Frequency-Division Multiplexing (OFDM), Multiple-Input-Multiple-Output (MIMO), Non-Orthogonal Multiple Access (NOMA), and Artificial Intelligence (AI)-based techniques have also been added. More details can be found in the Technical Consideration Document (TCD) of TG7a [13].

OCC distinguishes itself from other OWC technologies by applying a camera as the receiver. Several papers have already demonstrated comprehensive comparisons among OCC and other OWC technologies, and interested readers are recommended for more details in [3]. As OCC is treated either as an extension or as a subset of VLC in some literature [4], [5], [6], [18], to avoid confusion, OCC is seen as a camera-based OWC technology with VLC as a Photo Detector (PD)-based one.

Three basic components form a typical OCC system, namely, the transmitter, the optical channel, and the camera receiver as shown in Fig. 1. OCC can be divided into three categories based on different transceiver pairs. The combination of a single LED transmitter and a camera receiver (LED2C) is the first category.

An LED array transmitter and a camera, known as LEDA2C or visual MIMO form the second OCC category. The third type includes a screen transmitter and a camera (S2C) [5]. In this paper, we especially focus on the first two OCC categories.

III. Common Components, Main Parameters, and Analytical Models for OCC Systems

A. LED-Based Transmitter

1) Principles and Common Transmitter Sources for OCC Systems: Through recombination of the electrons and holes, LED provides illumination with the help of the intrinsic photon-generating nature and parasitic capacitance and inductance [22]. In the OCC field, LED illumination intensity, colour, and frequency can be modulated to carry information.

Three LED-based components are often applied as the transmitter in the existing OCC investigations. The first component comes from the LEDs of existing infrastructure, such as the traffic lights, advertisement panels and vehicle illumination lights. This type of LED is often applied to test the applicability of OCC in practical scenarios, such as the OCC-based Vehicle-to-Vehicle (V2V), Vehicle-to-Infrastructure (V2I), and Infrastructure-to-Vehicle (I2V) situations [22]. The second component is suitable for IoT-based indoor scenarios including the neopixel LED array, LED strip, and portable LED array. Multiple LEDs are often used together to enhance the transmission data rate [23]. The third component is the specifically designed LEDs to help achieve the required communication performance, such as the rotary LEDs proposed by investigators from Japan [24], the newly developed OLED [25], and micro-LED array [26].

2) Main Parameters: Main parameters are introduced based on single LED and LED array respectively.

Single LED: Transmitted optical power, LED frequency response, and LED Lambertian order are the three main parameters that affect OCC communication performance. Luminous intensity from the photometry perspective is the parameter influencing the OCC illumination performance.

The transmitted optical power P_{t} indicates the total energy radiated from an LED and is a parameter from the radiometric perspective with the unit Watt (W). It has a great impact on the possible achievable transmission distances of OCC systems and influences the suitable threshold value applied in the demodulation process. The value of P_{t} can normally be acquired from an LED vendor datasheet. However, for the sake of more rigorous analysis, three calculation methods have been proposed in OCC investigations [22], [27], [28], [29]. The first method is presented from the theoretical perspective, where P_{t} is described as the integral of the energy flux Φ_e in all directions given as [27]

$$P_{\mathrm{t}} = \int_{\Lambda_{\min}}^{\Lambda_{\max}} \int_{0}^{2\pi} \Phi_e d\theta d\lambda, \tag{1}$$

where $\Lambda_{\min}$ and $\Lambda_{\max}$ are determined by the sensitivity curve of the image sensor. As it's normally difficult to get the precise value of the energy flux, the second method is therefore proposed based on the linear relationship between the LED injected current I and P_{t} within its linear working area. It is also the most commonly used method for calculating the optical power in simulated OCC systems. It is given as [22], [28]

$$P_{\mathrm{t}} = kI, \tag{2}$$

where the linear coefficient k can be fitted through experiments as illustrated in [28], in which its value is approximately 2 and the LED driving current is set as 75 mA. The third calculation method is derived depending on the current I-voltage V characteristic of LED, and can be given as

$$P_{\mathrm{t}} = \eta IV, \tag{3}$$

where η is the value of photoelectric conversion efficiency. The mathematical relationship between I and V can either be fitted by a third-order polynomial as in [22] or through the diode equation proposed in [29].

As the LED light usually experiences a transition period when being driven by its current, it equivalently shows certain finite electrical bandwidth [22]. This property can be described by its frequency response and may impose limitations on the allowable flickering rate. A practical frequency-sweeping method mentioned in [22] can be applied to get the various frequency response results and the modulation bandwidths (defined as the 3 dB bandwidth) of different LED transmitters. A simple model which demonstrates the intensity variation of the light output with the angular frequency at a specific modulated voltage can be adopted to predict the LED frequency response as proposed in [22]. And authors in [30] present an approximate LED impulse response model with the exponential signal varies with the 3 dB cutoff frequency.

Lambertian radiant order m, or Full Width at Half Maximum (FWHM) as another name, can be used to measure the LED divergence angle which significantly affects the received power distribution [31]. Through careful determination, it can help to alleviate transmission distortion. m is given by [31]

$$m = \frac{-\ln(2)}{\ln(\cos(\Phi_{1/2}))}, \tag{4}$$

where $\Phi_{1/2}$ is the transmitter semi-angle. Optical diffusers are recommended to help adjust the Lambertian beam in order to get a better communication performance in OCC.

As a great many OCC systems use the visible light spectrum, LED light source brightness needs to be carefully adjusted to provide a comfortable illumination experience. Besides, for the application of OCC in V2V scenarios, transmitters that can provide acceptable road illumination without causing interference to other road users are also of great significance [32]. Luminous intensity is used to measure this property with the unit Candela (cd). It can be directly measured using a light meter or simply by referring to an LED manufacturer [33]. The luminous intensity in an angle ϕ can also be calculated as [34]

$$I(\phi) = \frac{m+1}{2\pi} I(0) \cos^m(\phi), \tag{5}$$

where $I(0)$ represents the center luminous intensity of the LED transmitter, and ϕ is the angle of irradiance.

Apart from the LED parameters mentioned above, the physical diameter and the applied flickering rate of the LED transmitter should also be carefully selected for OCC systems design.

LED diameter value has a close relationship with its supported transmission distances, whereas the flickering rate affects the data rate and human eyes' comfort [33].

LED array: When an LED array is applied as the transmitter of an OCC system, it has some unique influential factors which include LED placement shapes, LED intervals, and LED overlapping situations. The impact of the LED placements in an LED array has been investigated in [35], where the performance of three representative placements has been analyzed, namely, the Matern HardCore Point process (MHCP), the Binomial Point Process (BPP), and the circular shape. Results showed that the MHCP configuration with a more uniform Signal-to-Noise Ratio (SNR) can achieve better performance. The influence of the LED intervals in an LED array has been studied in [36]. Such intervals have an impact on the optimal ratio of LED light to ambient light (L2A), where L2A helps bring about the lowest Bit Error Rate (BER) without changing the data rate [37]. An OCC system with overlapped imaging LEDs has been validated to have a lower BER performance under the same condition compared to the one without such an overlap [38].

3) LED Analytical Models and Related Characteristics: The most frequently applied LED model in the OCC field is a generalized Lambertian model [27], [31], [34], which describes the emission of an LED as provided in (5). This model fits the LED characteristics well under indoor application scenarios, such as modeling the LED bulb [39] and 64-neopixel LEDs [23]. Values of m are different for modeling a single LED and an LED array. According to [23], an individual LED represents a complete hemisphere with m closes to 1, whereas its value becomes 0.74 when it is applied to model an LED array with no diffuser. Besides, an airy diffraction pattern is also commonly applied in OCC to model the light fringes extending from the borders of objects. This phenomenon in the captured images is due to the wavelike nature of light [40]. Stray light, which is a form of interference in OCC systems, is modelled based on the Point Spread Function (PSF) as [41]

$$s(r_i) = \frac{1}{\sigma\sqrt{2\pi}} e^{-\frac{{r_i}^2}{2\sigma^2}}, \tag{6}$$

where r_i is the distance from the research point to the original point, and σ is the intensity coefficient of the stray light distribution.

In spite of the wide applications of the Lambertian model, it appears to be inappropriate for the transmitters applied in V2V scenarios. This is mainly due to the fact that the emission pattern of the vehicle's light is specially designed to meet the illumination standard of driving with special power distribution [32]. Several efforts have been made to study the impact of realistic light radiation patterns on vehicular OCC systems based on the traffic lights [22], headlamps [32], and taillights [42], [43]. Radiation patterns of both the high- and low-beam headlamps have been analyzed in [32]. The asymmetric illumination distribution pattern of the low-beam headlamp which is specially designed to offer adequate forward and lateral illumination leads to the asymmetric distribution of the power, and thus brings about the positions of the zones with the lowest BER (formed by the BER contour lines) incline to be more skewed to the right. However, the radiation patterns of the high-beam headlamps and the taillights [42] are both more symmetric. The piecewise Lambertian model is used to estimate the radiation pattern of a scooter taillight, and the drastic shift in the trend of changes in the received power with respect to the transmission distance helps to indicate the irradiance angle of the scooter taillight [43]. The delivery capability of a transmitting LED traffic light associated with a beam-shaping lens is analyzed in [22] to perform link budget analysis. The discussions above on LED-based transmitters are summarized in Table I.

B. Optical Channel

1) Principles of Optical Propagation in OCC Channels: Line-of-Sight (LOS) links, Non-Line-of-Sight (NLOS) links, and a hybrid of them form the common transmission paths of OCC systems. For LOS links, the receiver directly acquires the transmitted messages from the transmitter. Comparatively, the receiver gets the transmitted messages after one or several reflections in NLOS links.

Indoor, outdoor, and underwater scenarios are the three typical channel environments in the OCC field. Communications between illumination lights on the ceiling and handheld smartphones, and data exchanged between wearable devices [2] can both be realized in indoor scenarios. Both LOS and NLOS links have been thoroughly investigated for indoor scenarios [19]. Channel quality for an indoor environment is the best on average among the three. Angular rotation and the blooming effect are the two key factors that decrease the OCC performance for this condition. Vehicular and drones-based communications [44] can be achieved in outdoor scenarios. Most outdoor-based OCC systems only consider LOS links, and very few of them realize outdoor NLOS links aided by atmospheric absorption. Channel quality for an outdoor environment is located in the middle of the three. Power attenuation caused by long distances, mobility phenomena, and weather impacts, such as fog and turbulence, all decrease the outdoor OCC performance [20]. We treat both below-water and water-to-air links [45] as underwater channels in this paper for description convenience. Underwater channel quality is the worst as light propagation ability is severely restricted by the presence of solids and dissolved materials. Besides, water turbulence and bubbles may further deteriorate its link quality [46].

2) Main Parameters: Channel Impulse Response (CIR) $h(t)$, Channel Frequency Response (CFR), and channel Direct Current (DC) gain $H(0)$ are presented as follows.

CIR $h(t)$: The main characteristic of the optical channel can be described by determining CIR, which can provide all the statistics of the channel in the time domain [47]. According to [47], the total CIR at time t is the sum of responses from LOS links and reflections from NLOS links for the light source S and the receiver R, which can be expressed as [27], [47]

$$h(t, S, R) = h^0(t, S, R) + \sum_{q=1}^{\infty} h^q(t, S, R), \tag{7}$$

TABLE I
ATTRIBUTES OF OCC LED-BASED TRANSMITTERS

Components	**Name**	**Application scenarios**		**References**
	LED infrastructures	Vehicular communications		[22]
	Neopixel LED array, LED strip, etc.	IoT-based indoor scenarios		[23]
	Specially designed LEDs	Scenarios require specific illumination patterns and a high data rate		[24]–[26]
Parameters	**Category**	**Name**	**Aspects that are influenced**	**References**
	Single LED	Optical power	Distances and demodulation threshold	[22], [27]–[29]
		Frequency response	Maximum allowable flickering rate	[22], [30]
		Lambertian order	Received power distribution	[31]
		Luminous intensity	Illumination experience	[32]–[34]
		Physical diameter	LED distinguishability	[28]
		Flickering rate	Data rate	[33]
	LED array	LED placements	SNR	[35]
		LED intervals	BER	[36], [37]
		LED overlapping	BER	[38]
Models	**Name**	**Suitable scenarios**		**References**
	Lambertian	Lambertian LED sources and reflection from rough surfaces		[23], [27], [31], [34], [39]
	Airy diffraction pattern	Modelling wavelike nature of light		[40]
	PSF	Stray light		[41]
	Empirical models	Headlamp, vehicle taillights		[22], [32], [42]
	Piecewise Lambertian	Scooter taillights, etc.		[43]

where $h^0(t, S, R)$ is the LOS response, $h^q(t, S, R)$ is the light response which undergoes q reflections. $h^0(t, S, R)$ can be presented as

$$h^0(t, S, R) = \frac{1}{d^2} P_t A_{eff}(\psi) \delta\left(t - \frac{D}{c}\right), \tag{8}$$

where D denotes the transmission distance, $A_{\text{eff}}(\psi)$ is the effective area of the receiver, ψ is the incidence angle, and c is the speed of light.

Based on CIR, the Root Mean Square (RMS) delay spread can be determined to quantify the degree of time dispersion and the Inter-Symbol Interference (ISI). The channel's impact on the transmitted signal distortion can also be analyzed and alleviated.

CFR: CFR represents the channel behavior as a function of frequency, and it characterizes the communication channel in the frequency domain [48]. CFR is also the Fourier transform of CIR.

Channel DC gain $H(0)$: As the frequency response of the optical channel is relatively flat near DC [49], DC gain becomes the most frequently used parameter to identify the transmission power losses in the channel. The relationship between $h(t)$ and $H(0)$ is as follows

$$H(0) = \int_0^\infty h(t) dt. \tag{9}$$

3) Channel Analytical Models and Related Characteristics:
Analytical channel models: The basic OCC channel can be modeled as a baseband Linear Time-Invariant (LTI) system with input $X(t)$ and output $Y(t)$ as [41], [47], [49]

$$Y(t) = \xi X(t) * h(t) + N(t), \tag{10}$$

where $*$ denotes convolution operation, ξ is the sensitivity of the camera image sensor with the unit (A/W), and $N(t)$ is the noise that can be modeled as Additive White Gaussian Noise (AWGN).

The channel path loss model, which is associated with the relationship between the received optical power and the transmitted one, can be modeled with the Lambertian, linear, exponential, and two-term exponential fittings according to [50]. Many commercial lighting LEDs without any beam shaping methods can be treated as Lambertian sources, and the channel path loss for them can be written as [51]

$$H(0)_{\text{generalized}} = \begin{cases} \frac{(m+1)A_r}{2\pi D^2} \cos\psi \cos^m\phi, 0 \leqslant \psi \leqslant \psi_c \\ 0, \qquad\qquad\qquad\quad \psi > \psi_c \end{cases} \tag{11}$$

where A_r is the optical detector area, ϕ is the irradiance angle, ψ is the incidence angle, and ψ_c is the camera Field of View (FOV). Piecewise Lambertian is acquired from the modification of the Lambertian model for transmitters with the specially designed spatial distribution as [50]

$$H(0)_{\text{piecewise}} = \begin{cases} \frac{(m+1)A_r}{2\pi D^\gamma} \cos\psi \cos^m\phi, 0 \leqslant \psi \leqslant \psi_c \\ 0, \qquad\qquad\qquad\quad \psi > \psi_c \end{cases} \tag{12}$$

with the path loss coefficient changes from 2 in (11) to γ. The value of γ varies according to the incidences and transmission distances. The received power P_r can then be calculated by multiplying the transmitted power P_t with either $H(0)_{\text{generalized}}$ or $H(0)_{\text{piecewise}}$.

When the linear channel path loss model is applied, the relationship between P_r and P_t can be given by [52]

$$P_r = P_t(\alpha D + \beta), \tag{13}$$

where α and β are weather dependent coefficients. The exponential model in [53] is presented as

$$P_r = P_t A D^{-2B} e^{-\varepsilon D}, \tag{14}$$

where A is geometrical loss, B is the decaying factor, and ε is the weather-dependent extinction coefficient. This model is suitable for describing the weather-influenced optical channel,

such as the fog phenomenon. The two-term exponential model in [48] is illustrated as

$$P_{\mathrm{r}} = P_{\mathrm{t}}(a_1 e^{a_2 D} + a_3 e^{a_4 D}), \tag{15}$$

where a_1, a_2, a_3, a_4 are fitting coefficients.

Optical channel characteristics: For indoor scenarios, the impact of multipath propagation is of main concern. Parameters that indicate the degree of ISI, such as the RMS delay and mean excess delay are specially paid attention to. Channel characteristics of both the simplified point-source model and the practical cases with various numbers of LEDs are compared in [54]. Non-negligible differences in the spatial distribution of the RMS delay spread under the above-mentioned cases have been validated. Large variations in the received power as well as the delay spread properties in different user movement trajectories have been analyzed in [55]. The impact of nonideal sources, the presence of objects, and wavelength-dependent reflection characteristics of surface materials on the indoor channels are depicted based on channel DC gain and RMS delay spread in [56]. The impact of different types of reflections on the optical channel, namely, the diffuse reflection and the specular reflection are studied in [57]. Optical power distribution and some statistical analyses which include BER have been investigated in both the static and mobile user environment in [58]. Critical insights into the influences of multipath reflections on indoor channel links have been presented in [59] where BER and channel delay characteristics are discussed.

For outdoor application scenarios, as the data rate of most OCC systems is not too high [32], multipath propagation-caused ISI may not be a major concern. Parameters related to channel path loss are paid more attention to under outdoor channel analysis. For applications in Intelligent Transportation Systems (ITS), the impact of the road surface irregularity and the road reflections from nearby vehicles are studied in [48] and [60] respectively. Related conclusions indicate that the road irregularity may contribute to the sudden increase of the received power, and the road reflections can change the time dispersion characteristics of the channel. The relationship between the communication range and the BER performance is outlined based on the proposed road-surface reflection model when both the LOS and NLOS links are considered [32]. Besides, the experimental results shown in [60] manifest that cars making turns could also lead to a significant change in the received power. Vehicle motion characteristics of the V2I, I2V, and V2V scenarios based on optical flow measurements are characterized in [61]. Related channel impulse responses of V2V and V2I under both the cross-road scenario and metropolitan scenario are carefully analyzed in [62]. Moreover, communication-related characteristics, such as the channel length estimation [63] and the link duration which can be described through generalized Pareto distribution under V2V application conditions [64] have also been investigated. Environment condition also attenuates the received optical power and may restrict the OCC feasibility in outdoor scenarios. Fog and atmospheric turbulence on the optical channel for V2V communications have been investigated in [65]. Results show that heat-induced turbulence has little influence on the system, whereas fog attenuation decreases signal quality significantly. The smoke attenuation, which is independent of the wavelength, has the same order magnitude of the channel attenuation level compared with fog as illustrated in [66]. The scattering due to the sandstorm is proved to be beneficial for increasing the data rate in OCC systems [67], and the in-depth analysis of the temperature's impact on the Signal-to-Interference-plus-Noise-Ratio (SINR) and BER are presented in [68] as well. For underwater application scenarios, the impact of turbulence and bubbles is analyzed in [45], [46]. The discussions above on channel-based contents are summarized in Table II.

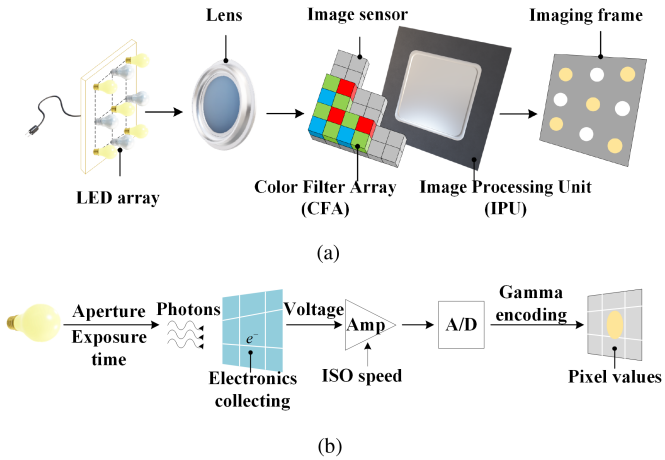

Fig. 2. Camera receiver illustration. (a) A brief imaging process which includes the schematic camera structure [6]. (b) A basic camera imaging process [33].

C. Camera as Receiver

1) Principles and Common Camera Components for OCC Systems: According to [6], a typical camera structure normally consists of an imaging lens, a Color Filter Array (CFA), an Image Sensor (IS), and an Image Processing Unit (IPU). A typical imaging process which includes the schematic camera structure is shown in Fig. 2(a). The basic imaging process of a camera can be described as follows. After the exposure time period, light received by the image sensor is sequentially transformed into photons, electrons, and voltages. Following the digitization process which takes place in Analog-to-Digital Converter (A/D), the final pixel value is acquired to be further processed to support the communication. The related process is shown in Fig. 2(b).

The image sensor is the core part of the camera that helps to sense light and realize imaging functionality. Charge Coupled Devices (CCD) and Complementary Metal Oxide Semiconductors (CMOS) are the two common image sensor types as shown in Fig. 3. The structure difference between CCD and CMOS is largely concentrated on their A/D part. The single A/D in CCD, to which the signal of each pixel needs to be serially transferred, greatly limits its supported frame rate. However, the delicately designed A/D for every column of pixels in CMOS helps to eliminate this bottleneck and helps support a higher data rate. Although CCD boasts of better imaging quality, the

TABLE II
ATTRIBUTES OF OCC CHANNELS

Environments	**Name**	**Impairments**		**References**
	Indoor scenarios	Angular distortion and blooming effect		[19], [44]
	Outdoor scenarios	Adverse weather, power attenuation and mobility		[20]
	Underwater scenarios	Bubbles and dissolved materials		[45], [46]
Parameters	**Name**	**Descriptions**		**References**
	CIR	Provide all the channel statistics		[27], [47]
	CFR	Provide channel frequency behavior		[48]
	DC gain	Identify channel path loss		[49]
Models	**Category**	**Name**	**Features**	**References**
	General models	LTI model	Baseband channel description	[41], [47], [49]
		Path loss model	Calculate the received power	[48], [50]–[53]
	Environment-based model	Indoor-related	ISI, RMS delay	[54]–[59]
		Outdoor-related	Power loss, weather effect	[32], [60]–[68]
		Underwater-related	Turbulence, bubbles	[45], [46]

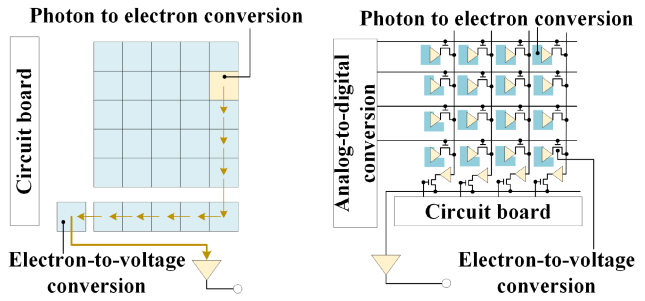

Fig. 3. Illustrations of CCD and CMOS [6]. (a) CCD. (b) CMOS.

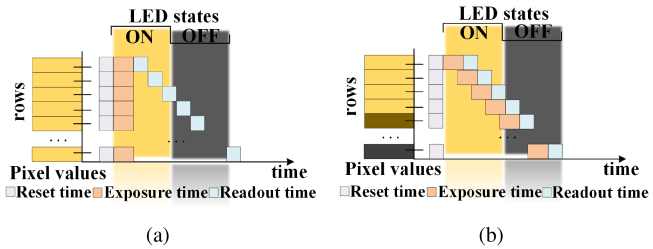

Fig. 4. Demonstrations of GS and RS modes. (a) GS mode. (b) RS mode.

advantages of the CMOS on faster readout and lower cost make it a better choice for OCC systems and therefore help it gains wider applications. There are two shutter mechanisms which include the Global Shutter (GS) and Rolling Shutter (RS) modes. CCD cameras often apply GS mode, in which all the pixels on the image sensor are exposed simultaneously. By contrast, CMOS cameras have the ability to support both GS and RS modes. As identical rows of pixels are exposed at the same time while adjacent rows experience a certain time shift, CMOS cameras with RS mode can help to achieve a higher data rate in OCC systems. Demonstrations of GS and RS modes are shown in Fig. 4.

Four types of camera receivers have ever been applied in OCC systems. The first camera type is off-the-shelf cameras such as smartphones and web cameras. They boast good integrations, medium supported frame rate (normally from 30 fps to 60 fps) and relatively high image resolutions. Besides, they are easy to implement in practical OCC systems without many modifications and are suitable for IoT-based indoor scenarios [16]. The second camera type is the industrial camera whose supported frame rate is up to 1000 fps [69]. They are suitable for application scenarios with strict real-time requirements. Event camera is the third type of camera receiver and its applications in the OCC field are located in the initial stage. Event cameras record changes in luminance in a pixel and output them as asynchronous events. Such characteristics help to acquire the data directly based on the generated events without image processing methods and are able to boost higher data rates with enhanced accuracy [24]. A specially designed camera such as Optical Communication Image Sensor (OCI) is the fourth type of OCC receiver to fulfill specific requirements. Other types of specially designed cameras include lensless camera, telephoto camera and multispectral camera [10], [70]. Due to their high performance, such cameras are usually cost-expensive [71].

2) Main Parameters: Three categories of camera main parameters are classified based on their impact aspects: communication speed-related, imaging intensity-related, and transmission distance-related.

The camera frame rate reflects the number of captured images per second and is measured with the unit frame per second (fps). It's the main parameter that limits the maximum supported data rate in OCC systems. The unique undersampled modulation formats in the OCC field are proposed to compensate for the low frame rate to avoid flickering. Camera frame rate variation is the main cause of the mismatch between the LED transmitter and the camera receiver in OCC systems, which may then lead to reception mistakes [72], [73]. Researchers in [72] investigated the frame rate variation with different image format outputs, and authors in [73] studied the theoretical bit error rate as a function of the related frame rate properties under the application of Undersampled Frequency Shift ON-OFF Keying (UFSOOK) protocol. Theoretical analysis for optimal synchronization has also been investigated in [74]. In most OCC investigations, researchers usually claim that the camera frame rate should be set

at least two times higher than the LED frequency rate to obey the Nyquist sampling theorem. Considering the fact that most of the OCC systems are used to transmit discrete digital signals such as binary 0-1 sequences instead of analogue continuous ones, this statement is not rigorous. When the transceiver is ideally synchronized, it's also possible to realize reliable communications when the OCC transceiver has the same frequency.

Camera exposure time, ISO, and lens aperture are the three parameters that help to determine how much light is received by the camera. Both the amount of the captured light and the camera's internal noises influence the LED imaging intensity. Camera exposure time controls the amount of light that reaches the image sensor and therefore helps to decide the brightness of the captured images. The study made in [75] illustrated that shorter exposure time within a certain time scope reduced BER under its experimental condition, whereas too long exposure time may lead to a blooming effect [76]. Shutter speed in some investigations is applied interchangeably with the exposure time, as the two parameters indicate the same camera property [77]. Besides, the camera shutter speed should also be more than twice the frame rate for secure communication as mentioned in [77]. ISO is used to measure the sensitivity of the image sensor. A higher ISO indicates faster absorption of the light and leads to an amplified image signal with increased noise levels [76]. The impact of an optimized one has been evaluated in [78]. The aperture or f-stop sets the amount of the captured light by the image sensor, which also influences the images' field depth. Studies in [76] and [79] demonstrated that a larger aperture leads to higher received power. Normally, an image sensor suffers from both signal-independent and dependent noises, such as ambient noise and temporal noise. Descriptions in [80] and [81] are recommended to learn more about the characteristics of camera noises.

Camera focal length influences the supported maximum distances. The larger the focal length, the longer the supported theoretical distance is. Basically, cameras work under the in-focus condition. However, there also exist application scenarios where cameras are presented to work under out-of-focus conditions with the aim of extending the transmission distance [79], [82]. Camera FOV is another significant factor that is determined by both the focal length and the sensor size [6]. Wider FOV has a larger tolerance for communications with mobility but imposes a limitation on the supported distance. A detailed theoretical model for the FOV as a function of both the distance and focal length has been reported in [83]. Researchers in [84] also study the impact of the image sensor resolution on the supported distances. Related results indicate that SNR drops with the increase in distance and resolution values.

3) Camera Analytical Models and Related Characteristics: Camera analytical models include two aspects which are imaging location determination and pixel intensity calculations. Geometric and radiometric camera models are proposed to realize the above-mentioned purposes respectively [85], [86].

Geometric camera models: The pinhole camera model is most frequently applied to describe the conversion process from the transmitters' physical coordinates (x, y, z) of the 3-Dimensional (3D) world coordinate system to their pixel coordinates (u, v) of the 2-Dimensional (2D) image coordinate system [28], [61], [86]. It can be expressed as [61], [86]

$$\mu \begin{bmatrix} u \\ v \\ 1 \end{bmatrix} = \begin{bmatrix} f & 0 & 0 \\ 0 & f & 0 \\ 0 & 0 & 1 \end{bmatrix} [\mathbf{R}\ \mathbf{T}] \begin{bmatrix} x \\ y \\ z \\ 1 \end{bmatrix}, \tag{16}$$

where μ is an arbitrary scale factor, f is focal length, $\mathbf{R}$ is a 3×3 rotation matrix, and $\mathbf{T}$ is a translation vector. For simplicity, the imaging radius is what the researchers especially pay attention to in some cases. Take the circular-shape transmitter LED with the physical radius of l as an example, the corresponding imaging radius l_i is calculated as [28]

$$l_i = \frac{lf}{D}. \tag{17}$$

The perspective projection [63], central projection [46], and trigonometric-based model [87] can also help to calculate the location of the imaging transmitter under static conditions. A pixel illumination model based on optical flow measurement proposed in [61] can be applied to describe the imaging positions of a moving transmitter for vehicular communications.

Radiometric camera models: A unified camera model with Mixed Signal-Dependent Gaussian Noise (M-SDGN) in the pixel-matched case is proposed in [81]. This model specifically considers the camera signal-dependent and signal-independent noises and is presented as

$$Z(t) = Y(t) + Y(t)Z_2 + \sqrt{Y(t)}Z_1 + Z_0, \tag{18}$$

where $Y(t)$ is the signal received by the camera after its transmission through the optical channel. $Z_0 \sim \mathcal{N}_{\mathbb{R}}(0, \zeta^2)$ is the signal-independent Gaussian noise with variance ζ. $Z_1 \sim \mathcal{N}_{\mathbb{R}}(0, b_1\zeta^2)$ and $Z_2 \sim \mathcal{N}_{\mathbb{R}}(0, b_2\zeta^2)$ are the signal-dependent shot noise and noise from Photo Response Non-Uniformity (PRNU) respectively. b_1 and b_2 are the ratios of the variances of Z_1 and Z_2 to the variance of Z_0. Based on the proposed model, the conditional Probability Density Function (PDF), SNR, and system capacity can be calculated.

A Linear Shift-Invariant (LSI) system was applied to simulate the RS-based CMOS cameras' working mechanism. Based on the LSI model, both the cameras' time domain and frequency domain characteristics can be described as [88], [89], [90]

$$Z(t) = Y(t) * h_{\mathrm{c}}(t) = A_{\mathrm{s}} \int_{t-T_{\mathrm{exp}}}^{t} Y(\tau)d\tau, \tag{19}$$

where T_{exp} is the camera exposure time, A_{s} is the scaling factor, $h_{\mathrm{c}}(t)$ is the camera impulse response calculated as

$$h_{\mathrm{c}}(t) = A_{\mathrm{s}}(u(t) - u(t - T_{\mathrm{exp}})). \tag{20}$$

Camera frequency response can then be illustrated as [88], [89], [91]

$$H_{\mathrm{c}}(\omega) = A_{\mathrm{s}} \frac{2\sin(\omega T_{\mathrm{exp}}/2)}{\omega} e^{-jwT_{\mathrm{exp}}/2}, \tag{21}$$

where ω is the angular frequency. If we assume the camera pixel is periodically sampled with period T_{cycle} and suppose the initial starting time is zero, the i-th sample produced by this LSI system

TABLE III
ATTRIBUTES OF OCC CAMERA-BASED RECEIVERS

	Name	Application scenarios	References
Components	Off-the-shelf cameras	OCC prototypes, mostly in indoor scenarios	[16]
	Industrial cameras	OCC applications with strict real-time requirements	[69]
	Event cameras	In need for higher data rate	[24]
	Specially designed ones	Applications with special necessities	[10], [70], [71]

	Name	Features	References
Parameters	Frame rate	Speed-related	[72]–[74]
	Exposure time	Intensity-related	[75]–[77]
	ISO		[76], [78]
	Aperture size		[76], [79]
	Camera noises		[80], [81]
	Focal length	Distance-related	[79], [82]
	FOV		[6], [83]
	Pixel resolution		[84]

	Category	Name	Features	References
Models	Geometric models	Pinhole camera model	Imaging location determination	[61], [86]
		Perspective projection		[63]
		Central projection		[46]
		Trigonometric relations		[87]
		Pixel model		[61]
	Radiometric models	M-SDGN model	Imaging intensity calculation	[81]
		LSI model		[88]–[90]
	Imaging model		Imaging process description	[28], [29], [33], [87]

can be presented as [88]

$$Z[i] = A_{\mathrm{s}} \int_{iT_{\mathrm{cycle}}+T_{\mathrm{rst}}}^{iT_{\mathrm{cycle}}+T_{\mathrm{rst}}+T_{\mathrm{exp}}} Y(\tau)d\tau, \tag{22}$$

where T_{rst} is the time duration a camera needs to start a new sampling process.

Based on the above-mentioned LSI-based camera model, investigators in [88] calculate the optimal exposure time for each sample and explore the clock-jitter effect that frequently happens in CMOS camera receivers. The relationship between the exposure time and the camera bandwidth was analyzed in [89]. Moreover, researchers in [90] study the camera's frequency response and internal noise characteristics by treating it as a Real-Time Oscilloscope (RTO). Other forms of the cameras' impulse response such as the Gaussian Point-Spread Function have also been presented in [92]. The LED images received at any other desired distances can then be estimated according to the Gaussian Mixture Model (GMM) applied at a reference distance. Moreover, the captured images can be modeled based on a signal layer and a texture layer [93].

There also exist other radiometric camera models which concentrate on describing the detailed camera imaging process which include photons collection, voltage transformation, amplification, digitization, and Gamma encoding [87]. Researchers in [33] present a method that is able to calculate the pixel value derived from the LED luminous intensity based on camera exposure settings. Different from [33], investigators in [29] especially consider the dimming control aided by Pulse Width Modulation (PWM) and demonstrate the relationship between its duty cycle and the LED luminous intensity. As the LED driving current can be better adjusted quantitatively to meet the communication requirement, [28] proposed a more detailed mathematical description to provide the validated relationship between the driving current and the image sensor pixel values under many application scenarios. The discussions above on camera-related contents are summarized in Table III.

IV. OCC Systems Implementation and Evaluation

A. OCC Systems Implementation

Experimentally set up OCC platforms and simulated OCC systems are two methods for investigating OCC. The former method can reflect OCC performance in realistic scenarios and provide OCC prototypes to further stimulate its practical applications. Simulation methods are beneficial in realizing systematic and intensive analysis of OCC performance while avoiding tedious experimentation campaigns. Implementation procedures for these two methods are introduced respectively as follows.

1) OCC Experimental Platforms Implementation: A completed data transmission process is demonstrated in Fig. 5. First, the transmitted data should be acquired. There are three common types of data sources for OCC experimental platforms: sensors which collect real-time data in IoT scenarios, computer-generated data bits, and signals from a signal generator. Next, coding and data encapsulations are implemented to help form data frames. Modulation techniques are then applied to transform these data frames suitable for transmission in optical channels. In practical OCC systems design, coding and modulation are often realized with the help of a Micro-Controller Unit (MCU) or highly integrated Field Programmable Gate Array (FPGA). As LEDs are normally applied as OCC transmitters, they should be guaranteed to use within their linear working regions. A Bias-T or triode-based circuit is then designed to fulfill

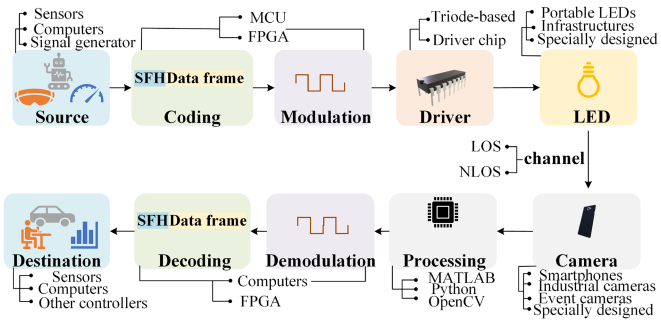

Fig. 5. Data transmission process on an OCC experimental platform.

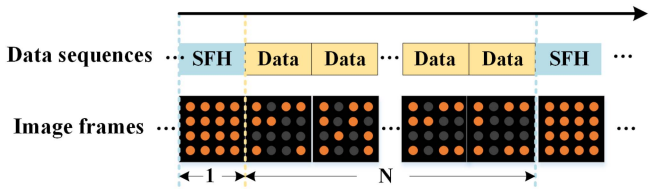

Fig. 6. Data frame design for realizing frame synchronization.

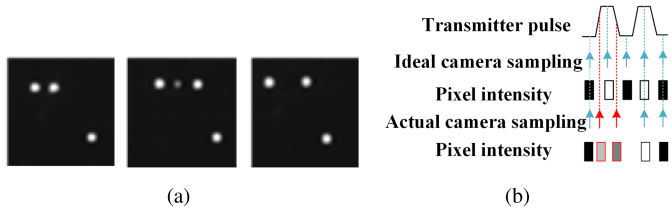

Fig. 7. Loss of the OCC bit synchronization. (a) Captured images under loss of bit synchronization. (b) Loss of bit synchronization caused by camera frame rate variation.

this condition. Dedicated chips are also good options to help drive large-scale LEDs simultaneously. After the electro-optical conversion at the LED-based transmitters, data then transmits through the optical channel. LOS links can be achieved as long as the transmitter is within the receiver's field of view. NLOS links can be achieved by placing an observation plane in front of the camera receiver and making it receive the information from the plane instead of directly from the transmitter. Besides, atmospheric scattering and absorption can also be depended on in outdoor scenarios to realize NLOS link data transmissions. As cameras record information based on the captured images, image processing-related techniques are applied based on MATLAB, Python, or OpenCV to recover the transmitted data. After demodulation and decoding procedures, the recovered data are finally acquired by the sensors or other controllers to realize communication.

For the sake of realizing the entire data transmission process, four key technologies which include synchronization, modulation, coding, and image processing should be paid special attention to.

Synchronization: OCC is a unidirectional technology, and synchronization can help the transceiver to stay in time sync. Frame and bit synchronization are two common synchronization schemes for OCC systems. Determining the beginning of a data frame is key to realizing frame synchronization. A Special Frame Header (SFH) can be inserted in front of every N data frames to help realize frame synchronization as shown in Fig. 6. By detecting the SFH and the number of received images between two SFHs, the receiver is able to judge whether a new data frame block starts and whether there are any missing data frames respectively. Based on the frame synchronization, bit synchronization needs to be further fulfilled to guarantee the camera sampling time coincides with the data transmission frequency. In other words, the start time of the camera exposure for each image within the two synchronized SFHs should be equivalently distributed, otherwise, the transition states of the LEDs may be captured which confuses their status determination. One such example is shown in Fig. 7(a), where the transition status of the middle LED in the first row is captured. Frame rate variation and the unavoidable time gap between the two consecutive frames of a camera receiver are the two main factors to cause bit asynchronization. The negative impact of the frame rate variation is demonstrated in Fig. 7(b). Repetitive transmission of the data frames and specially designed frame structures, such as the head-to-tail loop structure mentioned in [94] are the two common methods to compensate for the loss of bit synchronization. Besides, utilizations of the transceiver based on the same clock sources can be implemented to strictly guarantee time synchronization [95].

Modulation: Modulation is applied to change the data into forms that are suitable for transmissions in the optical channel based on Intensity Modulated (IM) /Direct Detection (DD). LED light intensity, frequency, colour, and spatial location can be modulated to carry information. IEEE 802.15.7 series of standards listed several modulation formats that are recommended for applications in different PHY layers for various scenarios. Besides, non-standard modulation techniques can also be referred to in [4]. For practical OCC systems design, the applied modulation methods are suggested to choose based on the utilization motivations. For the realization and testing of basic OCC prototype systems, ON-OFF-Keying (OOK) is suggested to apply due to its simple implementation. For balancing relationships between the relatively low frame rate of the cameras and the required LED flashing frequency, undersampled series of OCC modulations, such as UFSOOK [96] and hybrid modulations, such as Dimmable Spatial 8-Phase Shift Keying (DS8-PSK) [20] can be considered to avoid the flickering effect. To further enhance the supported data rate and increase the spectrum efficiency, higher-order modulations, such as PWM [71] and Variable Pulse Position Modulation (VPPM) [4] are recommended. A comprehensive summary of OCC modulations can be seen in [4].

Coding: Coding in the OCC field is applied to improve system reliability, extend the transmission distance and realize dimming control. Principles of coding are based on creating the mathematical relationship among the transmitted codes to facilitate the above-mentioned purposes. Similar to their applications in the RF field, rateless code and random code can be applied in OCC systems to increase the system reliability to help realize both

error detection and correction to some extent. Spatial coding methods are suggested to apply in the OCC field to combat LED distinguishability attenuation under long transmission distances, such as the proposed hierarchical code [97] and onion code [98]. They are also able to alleviate the negative interference of transceiver orientation. Dimming control aided by coding can be realized from two aspects. One is to balance the number of 1 and 0 in the original data sequence. The other is to avoid the existence of a long data string of 1 and 0. Application of the Manchester code is one such case to help realize dimming control. [5] is recommended for the systematically summarized coding schemes in the OCC field.

Image processing: As OCC systems use cameras as receivers, the locations of the transmitter LEDs and their information-carrying features are recorded in the form of images. Acquisition of the transmitted data relies heavily on image processing techniques whose performance influences the OCC communication quality to a large extent.

Off-line and online are two modes of image processing for OCC systems. The off-line mode is the most frequently applied one and it does not put strict requirements on the processing speed of the techniques. For this mode, images captured by the cameras are stored in a file which image processing schemes will later read from to acquire their input. For the online mode, the captured images will be processed in time once they are generated by the cameras. For some online OCC systems, image processing techniques are implemented on computers with an image capture card to support higher data transmission rates and reliability. Basic OCC image processing procedures are as follows. Input images experience preprocessing first which normally includes grayscale conversion, image denoising, enhancement, and binarization. Some necessary morphological operations may also be taken in some cases to facilitate the following procedures. Then, Region of Interest (RoI) areas candidates are selected based on two categories of methods [20]: one is based on traditional detection methods, such as the Hough circle detection and projection method which normally depend on the intensity and geometric features of transmitters; the other is based on the advanced computer vision-related DL schemes, such as the You Only Look Once (YOLO) detection network. Next, the tracking algorithms are applied to further determine the targeted transmitter to help set up and remain communication links. Similarly, there also exist traditional tracking methods, such as the template matching method, optical flow method, and frame difference method, together with DL-based tracking methods, such as the Tracking-Learning-Detection (TLD) method. Normally, the transmitter imaging area is detected as a whole. For transmitters with multiple LEDs, the imaging area of each individual LED needs to be further selected. Finally, LED states with information-carrying features are acquired according to the preset-related threshold.

Two aspects need to be paid special attention to for the OCC image processing. Threshold selection is the first aspect, which influences the accuracy of binarization and LED status determination. The threshold for binarization is used for the elimination of background noises, such as the camera's internal noises. The value of this threshold has a great relationship with the environment illumination and can be estimated based on the dark

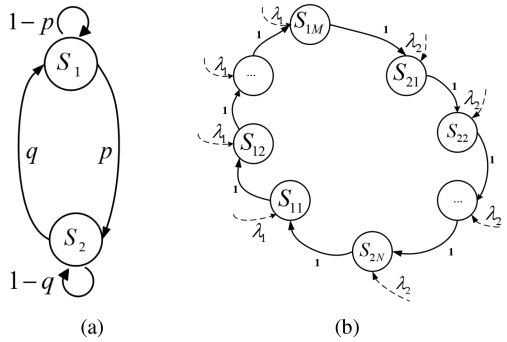

Fig. 8. The analytical model for the RSE-based camera capturing process. (a) Gilbert-Elliott model. (b) The MMBP model.

frames. Pixel value variation, blooming effect and interferences from the adjacent LEDs all interfere with the threshold selection for LED status determination. Values of this threshold can be estimated based on the known preamble sequences, and multiple thresholds can be allocated to different imaging areas of the same image to further enhance the accuracy. Techniques selection for LED detection and tracking is the second aspect. Accuracy and time complexity need to be balanced based on the application scenarios. Traditional detection and tracking method can be applied when the communication background is simple. Besides, considering the sparse features of LED transmitters, classical DL-based networks can be further optimized to increase the processing rate.

2) OCC Simulated Systems Implementation: There are two categories of simulated OCC systems, one is concentrated on the data packet-based performance investigations which are similar to those made for packets in the computer network, and the other puts more emphasis on OCC synthetic images-based research.

Data packet analysis-based OCC simulated systems: This category is for the sake of simulating OCC systems with the Rolling Shutter Effect (RSE). When the LED flashing frequency is greater than the frame rate but lower than the camera row scanning frequency, RSE occurs as the data is received in the form of a series of dark and illuminated stripes in the captured images. The analytical model applied for imitating the camera capturing process is key to implementing such OCC simulations. Based on whether the camera is in its capturing time or in its inter-frame time, the Markov chain can be intuitively applied as the OCC system model, such as the two states Gilbert-Elliott model as shown in Fig. 8(a) and the more accurate Markov-Modulated Bernoulli Process (MMBP) as shown in Fig. 8(b). In Fig. 8(a), state S_1 means the OCC system is capturing a frame whose reception probability is $1 - P_e$, where P_e is the packet decoding error probability. State S_2 means the camera is not capturing any images and its reception probability is 0. The transition probability between S_1 and S_2 is p, and probability between S_2 and S_1 is q. Values of p, q are calculated as the function of inter-frame gap δ_g, frame duration δ_c, and camera capture time δ_f. They are also assumed as constant and are independent with P_e. Calculation of p and q is given as

$$p = 1 - q = \frac{\delta_f - \delta_g}{\delta_f} = \frac{\delta_c}{\delta_f}. \tag{23}$$

Considering the fact that transition probability from one state to another depends on its residence time and is not always deterministic, the MMBP model is proposed where a total number of $M+N$ states representing the reception of a packet are considered. As shown in Fig. 8(b), M states correspond to camera capture time and N states correspond to inter-frame time. Here, as discussed before, λ_1 is the arrival rate with the value $1-P_e$ and λ_2 is 0. The value of $M+N$ states is influenced by the LED imaging area. To be more specific, the ratio between the LED imaging area and the captured image size equals the ratio of M states in the $M+N$ states and is the function of the distance, LED size, camera sensor size, and camera focal length. Based on these analytical models, the successful probability of receiving a data packet can be calculated, and system performance such as throughput and BER can be acquired. More implementation details of such simulation can be found in [99].

Synthetic image analysis-based OCC simulated systems: Synthetic images are generated in this category of OCC simulations based on multidisciplinary knowledge related to photometry, camera geometry, and digital image acquisition. Simulations of both RSE-based and non-RSE-based OCC systems are investigated [100], [101]. Procedures for the generation of synthetic images are as follows. First, system parameters need to be selected based on communication requirements, such as the LED optical power and illumination pattern, optical channel distance and environment, camera focal length, frame rate, and exposure time. Descriptions of OCC system key parameters and their modeling methods can be found in Section III. Then, the LED imaging area needs to be determined. For non-RSE systems, individual LED is treated as a basic reception unit, and its corresponding imaging coordinates can be calculated based on (16). As most of the existing OCC simulations suppose the transceiver are parallel to each other and the transmitter is assumed to be imaged in the central area of the image sensor, calculation of LED imaging radius in (17) is of more concern. For RSE-based systems, the width of the dark and illuminated stripes needs to be further calculated. Assume the LED flickering frequency is f_{LED} and the camera row scanning frequency is f_{scanning}, the theoretical row number $n_{\mathrm{stripe\_row}}$ each imaging stripe takes is calculated as

$$n_{\mathrm{stripe\_row}} = \frac{f_{\mathrm{scanning}}}{f_{\mathrm{LED}}}. \tag{24}$$

Given the vertical resolution $h_{\mathrm{ver\_reso}}$ which is also the total number of rows in an image, the formed stripes quantity $h_{\mathrm{stripe\_num}}$ is calculated as

$$h_{\mathrm{stripe\_num}} = \frac{h_{\mathrm{ver\_reso}}}{n_{\mathrm{stripe\_row}}}. \tag{25}$$

Next, pixel values of the imaging LED need to be determined. Driving current-based, luminous exposure-based, and a rule of thumb-based exponential function calculation methods can be applied to calculate the corresponding pixel values. Finally, the background noises are required to be added before the final synthetic images are obtained. Camera noises such as a fixed Gaussian noise can be added to the image to approximately simulate channel and camera internal noises. A predefined camouflage image may also be overlayed on the generated one to simulate real-world background [102].

Apart from the above-mentioned descriptions of the basic transmitter imaging, more advanced theories such as tensor [103], Markov chain [104], high-order statistics [105], and Computer Vision [106], [107] are applied to simulate unstable camera frame rate, terminal jitter, system asychronization, and mobility-induced angular distortion which are closer to realistic communication conditions.

B. OCC Systems Evaluation

Communication speed, distance, quality, and reliability-related OCC systems evaluation are presented.

1) Communication Speed Evaluation: The raw data rate, throughput, and system capacity are three communication speed evaluations in the OCC field. Raw data rate indicates the total received bits per second. It can be obtained by measuring the data received within a given time period in a practical system. It can also be theoretically calculated by multiplications of channel per frame and frame per second. Channel per frame for OOK-based non-RSE systems is the number of transmitter LEDs in each image. For RSE systems, it's the multiplication of the transmitter LED number and imaging stripe-based data bits carried by each LED. The communication speed of OCC systems ranges from bps for indoor IoT-based scenarios to Mbps for outdoor V2V-based scenarios [12]. If the effective transmission speed (the received information-carrying bits per second) is in demand, throughput is the required criterion [108].

System capacity is used to measure the data transmission potentiality of OCC systems, and it can be derived from the modified Shannon's capacity formula. According to [77], [109], perspective distortions and characteristics of AWGN both deteriorate OCC system capacity. One calculation method can be used to approximate the capacity of nonnegative channels in OCC systems as [77]

$$C_{\mathrm{OCC}} \approx W_{\mathrm{fps}}(W_{\mathrm{s}}\log_2(1+\mathrm{SINR})), \tag{26}$$

where W_{fps} is the camera frame rate, and W_{s} is the spatial bandwidth which is equivalent to the number of orthogonal or parallel channels in a MIMO system, and SINR is the Signal-to-Interference-plus-Noise-Ratio. Typical value of C_{OCC} ranges from 10^4 bps to 10^5 bps for an OCC system with 100 fps camera.

2) Distance Evaluation: The supported distance of an OCC system is the maximum distance achieved when the system can provide reliable data transmission. Normally, an OCC system is treated as reliable when its BER is below the Forward Error Correction (FEC) threshold (3.8×10^{-3}). Supported distances of OCC systems range from a few centimeters in indoor scenarios up to 400 meters in outdoor scenarios when the camera works in the out-of-focus mode [82].

3) Quality Evaluation: Qualities of the communication environment and captured images are two aspects of OCC quality evaluation. SNR and SINR are applied to measure the former aspect, and the Peak-Signal-to-Noise Ratio (PSNR) is used to evaluate the latter aspect.

SNR can be calculated based on three calculation methods. The first method is based on the pixel photocurrent [65], [78]. One of its common expressions can be presented as [78]

$$\mathrm{SNR}_{\mathrm{current}} \approx \frac{i_{\mathrm{pd}}(u_{\mathrm{c}}, v_{\mathrm{c}}, ch) \cdot G_{\mathrm{V}}^2}{G_{\mathrm{V}}^2} \cdot (\sigma_{\mathrm{th}}^2 + \sigma_{\mathrm{sh}}^2) + \sigma_{\mathrm{adc}}^2, \tag{27}$$

where $(u_{\mathrm{c}}, v_{\mathrm{c}})$ indicates the camera pixel position, ch belongs to one of the R, G, B channels, and G_{V} is the camera gain of the analog amplifiers. σ_{th}^2 and σ_{sh}^2 indicate the camera thermal noise and shot noise respectively. σ_{adc}^2 is the noise induced by A/D, which can be virtually reduced to zero by increasing the value G_{V}. The second method is based on the received optical power [32], [81], [110], [111]. Normally, the received optical power P_{r} is calculated through the channel DC gain $H(0)$. One of its typical representations can be shown as [110]

$$\mathrm{SNR}_{\mathrm{power}} = \frac{P_{\mathrm{r}}^2}{\sigma_{\mathrm{total}}^2} = \frac{P_{\mathrm{t}}^2 H^2(0)}{\sigma_{\mathrm{total}}^2}. \tag{28}$$

The third method is a unique approach in the OCC field. It calculates the ratio of energy per bit E_b and noise spectral density N_0 on the image sensor of a camera as [6]

$$\frac{E_{\mathrm{b}}}{N_0} = \frac{E[PV^2]}{E[n^2]} \approx \frac{a^2 T_{\mathrm{exp}}}{g_1 a T_{\mathrm{exp}} + g_2}, \tag{29}$$

where PV is the pixel value, a is the amplitude of light, n is the noise value, g_1 and g_2 are noise model fit parameters.

In summary, OCC signal-to-noise intensity normally ranges from -10 to 90 dB, and can be calculated based on $\mathrm{SNR}_{\mathrm{current}}$, $\mathrm{SNR}_{\mathrm{power}}$, and $\frac{E_{\mathrm{b}}}{N_0}$ with different description emphasis. Among them, the first two methods calculate such intensity which treats the sensor as a single unit based on current and power respectively, whereas the third method provides a more specific approach which treats each pixel on a sensor as a single unit.

SINR is applied to measure the interference impact and normally ranges from 0 to 85 dB. Two types of interference sources have been considered in the existing OCC investigations. For RSE OCC systems, the impact of the adjacent imaging dark and bright stripes-based interference can be described as [33]

$$\mathrm{SINR}_{\mathrm{stripes}} = \frac{\sum_{u=1}^{h_{\mathrm{t}}} PV_u + h_{\mathrm{b}} \cdot PV_{\max}}{\sum_{u=1}^{h_{\mathrm{t}}} PV_u + h_{\mathrm{b}} \cdot PV_{\min}}, \tag{30}$$

where $PV_{\max}$ indicates the maximum pixel value corresponding to the rows that are fully illuminated by the LED light and ambient light during the exposure period. $PV_{\min}$ denotes the minimum pixel value corresponding to the rows that do not receive any LED light. h_{t} is the height of the transition band, and h_{b} is the height of the complete white (or black) band. For LED array-based non-RSE systems, the impact of the interference generated by the neighboring light sources can be obtained as [41], [77]

$$\mathrm{SINR}_{\mathrm{adjacent\_LEDs}} = \frac{(1-\chi)P_{\mathrm{r}}^2}{P_{\mathrm{adjcent\_LEDs}}^2 + P_{\mathrm{noise}}}, \tag{31}$$

where χ is defined as the image distortion factor.

PSNR is calculated as [6], [23], [82]

$$\mathrm{PSNR} = 10\log_{10}\left(\frac{PV_{\mathrm{input\_max}}^2}{\mathrm{MSE}}\right), \tag{32}$$

where $PV_{\mathrm{input\_max}}$ is the maximum span of input data (e.g., for 8-bit cameras, the value of $PV_{\mathrm{input\_max}}$ is 255). MSE is the mean squared error between the transmitted and the received images.

4) Reliability Evaluation: BER, Packet Error Rate (PER), and Symbol Error Rate (SER) can be applied to measure the reliability of OCC systems from the perspectives of bit, data frame, and symbol respectively. They can either be directly obtained by measuring the proportion of those falsely received data bits, frames, and symbols in the systems' totally received ones or be calculated theoretically. When OOK is applied, theoretical BER can be calculated as [112]

$$\mathrm{BER} = \frac{1}{2} e^{-\frac{\mathrm{E_b}}{\mathrm{N_0}}}. \tag{33}$$

For other higher-order modulations, BER can be obtained with the help of the Q function which is similar to the one provided in the RF field as mentioned in [32] and [110]. PER and SER are normally applied in practical application systems, such as V2V links in outdoor scenarios [83], [113]. One typical PER expression is presented in [83] as

$$\mathrm{PER} = 1 - (1 - Q(\sqrt{\mathrm{SNR}}))^N, \tag{34}$$

where N represents the bits number in a data packet. The discussions above on OCC systems evaluation criteria are summarized in Table IV.

V. OCC Systems Performance Enhancement Solutions

A. Improve the Communication Speed

In the OCC field, as the received data bits are acquired based on the captured images, two aspects are frequently considered to improve the data rate. One is by improving the number of captured images per second, the other is by increasing the carrying bits number per image.

Increasing the camera frame rate is one direct method to improve the captured images per second. Correspondingly, for those online-processing OCC systems, the required image processing time needs to be decreased to avoid data dropout as well. With the help of high frame rate cameras (beyond 1000 fps) [69] and the delicately designed image sensor [71], a data rate of up to 10 Mbps OCC system can be achieved even in outdoor scenarios. Application of new camera types, such as event cameras [24] can also be considered to enhance the data rate as they can asynchronously output changes in brightness as events in microsecond order. Another solution is realized by reducing the image processing area to indirectly increase the equivalent camera frame rate. RoI [20] and Selective Capture (SC) [114] are two typical proposed schemes within this scope. For the RoI scheme, once images with full resolution are captured, RoI is first determined based on object detection methods, such as the frame difference method [69] and DL-based ones [20], [115]. Then, image processing-based techniques are applied only on the selected RoI areas instead of the full images to reduce the

TABLE IV
OCC SYSTEMS EVALUATION CRITERIA

Category	Criteria		Descriptions	Range	References
Speed	Raw data rate		Totally received bits per second	From bps up to Mbps	[12]
	Throughput		Received information-carrying bits per second	From bps up to Mbps	[108]
	C_{OCC}		System capacity	10^4-10^5bps for 100 fps cameras	[77]
Distance	Distance		Maximum supported reliable distance	From cm up to 400 m	[82]
Quality	SNR	$\mathrm{SNR}_{\mathrm{current}}$	SNR based on pixel photocurrent	-10-90 dB	[78]
		$\mathrm{SNR}_{\mathrm{power}}$	SNR based on optical power		[110]
		$\frac{E_{\mathrm{b}}}{N_0}$	SNR for an individual pixel		[6]
	SINR	$\mathrm{SINR}_{\mathrm{stripes}}$	Interferences from adjacent imaging stripes	0-85 dB	[33]
		$\mathrm{SINR}_{\mathrm{adjacent\_LEDs}}$	Interferences from adjacent imaging LEDs		[77]
	PSNR		Captured image quality	0-3.5 dB for 150-400 m	[82]
Reliability	BER		Bit error	Below FEC threshold	[112]
	PER		Packet error		[83]
	SER		Symbol error		[113]

processing time. In contrast, for the SC scheme, only areas with the imaging transmitter LEDs are captured for further processing [114].

For improving the carrying bits number per image, one direct solution is to increase the number of transmitter LEDs. LED array [23], rotary LED [24], and Red-Green-Blue (RGB) LED [116], [117] can be applied to achieve this goal. Besides, as RSE [30] allows multiple data bits transmitted in various periods to be recorded within one image, it can be applied to further improve the bit-carrying ability of the individual LED as long as two requirements are met: one is the camera needs to be working under RS mode, and the other is the LED flickering rate needs to be higher than the camera frame rate but lower than its row scanning frequency. Enlarging the LED's physical size and suitably improving its flickering rate can further increase the carrying bits per image, as both two ways can help improve the number of data-carrying RS stripes. High-order modulation is another solution. PWM [71], [118], Composite Amplitude Shift Keying (CASK) [108], OFDM [69], and CSK [113], [119] are some of the typical modulation formats ever used in the OCC field.

B. Extend the Distance

The intensity of the captured images, the size of the LED imaging area, and the distinguishability of LEDs all interfere with the achievable transmission distance. Compensation for the attenuation of the received optical power, enlarging the LED imaging area, and resistance of the captured image degradation are the three corresponding solutions. As RSE-based OCC systems are largely intended for short-distance OCC systems, distance-extending-based solutions only for non-RSE systems are presented here. Enhancement for RSE-based systems is described in the next part.

Three categories of methods can be used to compensate for optical power loss. Increasing the transmitted optical power is the first common and straightforward method [28]. However, restricted by the safety of human eyes and the harmful effect in some of the light spectrum, the maximum allowable optical power is limited. Alternatively, increasing the camera gain [78] is also beneficial to amplify the received optical power to some extent. Besides, relay-based schemes can also be considered to compensate for the power attenuation, such as applications of the mobile robot-based camera [111] and the LED-equipped drone [117].

Limited imaging area is another factor restricting the supported distance. Three methods can be applied to enlarge the imaging area. The first method is to increase the camera focal length [71]. The second method is to make full use of camera defocus mode which supports larger LED imaging areas. A maximum of 400 m OCC communication link is possible [82] based on this method. The third method is realized by spatial multiplexing based on coding where multiple LEDs are used to transmit the same data information and are treated as one OCC transmitter. Hierarchical coding [97], Alamouti-Type Coding [120], and Layered Space-Time Coding (LSTC) [121] are brought into the OCC-based communication systems to realize a transmission distance up to 155 m in V2V scenarios.

Loss of LED distinguishability is very common for MIMO OCC under long transmission distances. It is largely due to the diffusion of LED and the finiteness of the image sensor pixel size [71] which then leads to a phenomenon called InterPixel Interference (IPI) (in some studies, IPI and ISI represent the same). IPI cancellation schemes such as differential coding [122] and adaptive threshold detection method [123] can be applied to fight against the IPI of an LED array transmitter. Apart from the pixel intensity, some new specifically designed criteria are also explored to guarantee the OCC performance under low LED distinguishability. Image slope variation [124], [125], Average Grayscale Ratio (AGR), Gradient Radial Inwardness (GRI), Neighbour Grayscale Ratio (NGR) [40], and discrete Fourier transform [126] can be utilized to extend the OCC transmission distance with higher reliability. An error-free distance of the OCC-based vehicular network is able to be extended from 40 m to 60 m with the help of the above-mentioned schemes.

C. Increase the Quality

Optical channel environment, clarity of the captured images, and illumination comfort are the three aspects to evaluate the OCC quality.

Optical channel noises and camera internal noises are two common noise categories to deteriorate the quality of the OCC communication environment. Averagely speaking, the noises of CMOS cameras are more obvious than those of CCD cameras. As there is a lack of analytical models and characterizations of such noises, a neural network is suggested to alleviate their negative impact [127]. Strong sunlight in outdoor scenarios also deteriorates OCC system performance by leading to the overexposure of the captured images which threatens the transmitter detection. Reducing the amount of light entering the camera by decreasing its exposure time, ISO, and aperture size helps alleviate such a phenomenon. Besides, adding a light baffle at the transmitter end also helps.

Image blur is the main factor that interferes with image clarity. Camera defocuses, transceiver motion, and foggy weather all lead to blurry captured images. Maximum Likelihood Estimation (MLE) [128] and Maximum Likelihood Decoding (MLD)-based template matching [129] can be applied to realize deblurring. DL-aided deblurring algorithms [130], [131], [132] also work well for such a phenomenon. Besides, directly improving the camera frame rate help reduce the motion-caused blurry impact [28]. Recently, the selection of an appropriate image compression scheme has proved to be efficient in improving the image quality as well [133].

Avoiding the human eyes' perception of LED flickering is significant to realize illumination comfort in OCC systems. The LED flickering rate needs to be higher than the critical perceived frequency of human eyes (100 Hz) while also being able to match with the relatively low frame rate cameras. Undersampled modulations have the advantage of supporting OCC systems with data rates higher than the applied camera frame rate to avoid human eyes' perception of LED flickering. UFSOOK [19] is the first proposed undersampled modulation format in the OCC field with 0.5 b/frame/LED spectral efficiency. It employs two square-wave subcarriers at frequencies that are harmonics of half the camera frame rate to represent bits 0 and 1 respectively. Due to the specially designed relationship between the subcarrier frequency and the camera frame rate, when symbol 1 is transmitted, the two captured LED states during the symbol period which contains an odd number of square-wave cycles are different. However, the two captured LED states are identical when 0 is transmitted. Motivated by UFSOOK, a series of undersampled modulation schemes with improved spectral efficiency are proposed, such as Undersampled Phase Shift ON-OFF Keying (UPSOOK) [134] and Undersampled m-ary Pulse Amplitude Modulation (UPAM) [19]. Besides, many other uniquely designed modulation formats for OCC are proposed considering both the dimming level and the frame rate, such as VPPM, PWM, and Hybrid Spatial Phase-Shift Keying (HSPSK) [20]. Coding is another method to realize dimming control. One coding method is Manchester code which is able to balance the quantity of 1 and 0 as well as avoid their long consecution. DL-based AutoEncoder (AE) is another coding method to realize dimming support by adjusting the number of 1 in a binary codeword [135], [136].

D. Enhance the System Reliability

The angle distortion, interferences caused by adjacent stripes in RSE systems and neighbouring light sources in non-RSE systems, complicated background, as well as loss of synchronization all interfere with the OCC systems' reliability. Besides, transmission link security is also an important aspect which influences communication reliability.

As the OCC channel is not isotropic, when the transmitter LED and the camera receiver are not parallel to each other, angle distortion occurs which then leads to partial imaging or even blockage [137]. A clear definition of the camera angle is demonstrated in [138], where the effect of both the horizontal and vertical angles are thoroughly analyzed. Various solutions are recommended for RSE and non-RSE-based OCC systems to compensate for the power loss and imaging distortion caused by such a phenomenon. For RSE-based systems, a Pixel Rearrangement (PR) scheme can be applied to resist camera angular offset according to the imaging intensity with the Stripes Separation Logic Decision method (SSLD) [139]. Similarly, a row grayscale redistribution together with the packet selection method can be used to improve the OCC decoding accuracy under rotational and translational motions of the transceivers [140]. For non-RSE-based OCC systems, a special header frame can be proposed to support data receptions of multiple users at various orientations [141]. A hierarchical transmission scheme can also be considered to help reduce the computation complexity of rotation detection in LED array-based OCC systems [142].

Interference is another negative influential factor for OCC systems. For RSE-based OCC systems, two categories of interferences exist: one comes from the interference caused by the blooming effect of the adjacent imaging stripes, and the other is from the background layer below the imaging stripes. For the first type of interference, two solutions are recommended. The first solution category concentrates on alleviating the negative interferences caused by adjacent imaging stripes based on algorithms such as equalization method [143], artificial neural network-based method [144], [145], [146], and the ensemble averaging and selective reception method [147], [148]. The second category is to modify the selected threshold to combat interference. Bradley adaptive thresholding [149], entropy-based thresholding algorithms [150], and Extreme Value Averaging (EVA) [151] are introduced to adaptively cope with the ununiform distribution of the imaging pixel values. For the interferences caused by the imaging background such as the advertising and museum display poster in RSE-based systems, two categories of suggestions are recommended. The first category is aimed to directly cope with the background-included images with the help of algorithms such as the Extinction Ratio (ER) enhancement [152], Machine Learning (ML)-based logistic regression [161], the rearrangement of the Grayscale Value Distribution (GVD) [153], the modified background subtraction [162], and Deep Neural Network (DNN)-based method [154]. The second category is to detach the background with these data-carrying stripes and deal with them respectively to realize the functions of object detection and information acquisition. A disentangled representation learning-assisted method is

proposed in [155], where the Generative Adversarial Networks (GAN)-reconstructed background images and the residual of the original ones are acquired to realize the above-mentioned targets. For non-RSE-based OCC systems, interferences from the adjacent LEDs and the complicated background are also the two main interference sources. The first type influences LED distinguishability and has been discussed in the previous part. Compared with the background of RSE-based systems, non-RSE-based ones are more complicated due to the existence of more light sources together with other imaging objects due to various application scenarios. Besides, the LED imaging area is more limited as such systems normally support longer distances. To cope with such complicated scenarios, conventional image processing methods based on geological features, such as the isosceles triangle searching [156], and more advanced machine learning-based technologies for RoI determination, such as the CNN-based scheme [130], and You Only Look Once series (YOLO) object detection model [131], [157] are applied.

Loss of synchronization and packet dropout caused by inter-frame gaps and camera frame rate variation are other factors that interfere with the OCC systems' reliability. Utilizing a camera receiver with a relatively stable frame rate is an effective solution [72]. Data transmission based on repetitive schemes and spatial multiplexing are two ways to combat the inter-frame gap [97], [98]. A packet-reconstruction technique [94] and a stripe length estimation-based sampling scheme [158] are also able to support higher tolerance of both larger Sampling Frequency Offset (SFO) and more adverse effects of the frame gap time. Besides, camera exposure time synchronization is realized in [95].

Different from the above three aspects that degrade the system performance due to the transceivers' status and the quality of the channel between them, security is the one that relates to transceivers' legitimacy and determines whether the information can be received by the right user without eavesdropping. The unique location-aware ability of OCC can help realize a multi-channel authentication by integrating Diffie-Hellman key exchange [159]. A security protocol realized by the verification key transmitted by an OCC link [160] can also help to enhance the security of autonomous vehicle platooning. The discussions above on OCC systems performance enhancement solutions are summarized in Table V.

VI. OCC Systems Design Examples

A. Indoor OCC Experimental Platform Design Example

Our designed indoor OCC platform serves to present related technical details and OCC applicability for indoor scenarios as a prototype. For simplicity, the transceiver is assumed to be static and parallel to each other. Two typical indoor environments are considered which include the office room and corridors of the school building. The setup of the indoor OCC platform is presented in Fig. 9.

1) System Main Parameters and Implementation: Main parameters' values of the LED-based transmitter and camera receiver are presented in Table VI.

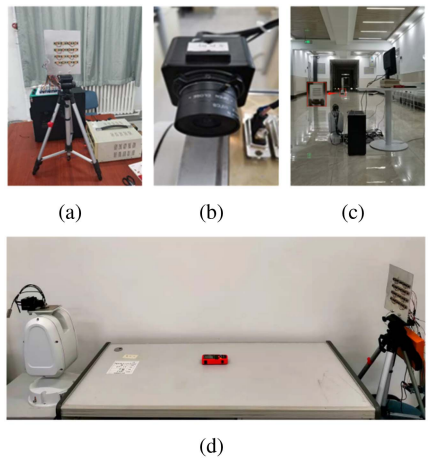

Fig. 9. The setup of the indoor OCC platform. (a) The 808 nm 4×4 LED array. (b) The camera receiver. (c) The indoor corridor environment. (d) The indoor room environment.

We use a computer to generate the transmitted data packet. There exist 57 images within one data packet, where the first 7 images with Barker sequences are used for frame synchronization. P2.0-P2.7 and P3.0-P3.7 ports of the MCU are applied to modulate the 16 LEDs. OOK is applied as the modulation format in our OCC system, and no coding mechanism is used. The triode-based circuit is applied to drive the LED array. LED driving current value is determined as 75 mA, under which the LED imaging spot is clear without a blooming effect. As the camera frame rate is 25 fps, the LED flickering rate is set as 12 Hz to avoid data dropout. Only LOS links are considered in our system and an 808 nm filter is added in front of the camera receiver to realize reception of the data-carrying-808 nm optical band. Universal Serial Bus (USB) is used to connect the camera to the computer used for Python-based image processing. As the application of the 808 nm filter decreases the negative impact of complicated background and reduces the requirements for the applied image processing techniques, the basic and simple projection method is able to accurately determine the imaging location of the LED array. The data bits are then retrieved based on the LED states according to the preset threshold. The acquired data bits are finally stored in a file for further performance evaluation and communication.

2) Design Challenges and Performance Achieved: Interference and blooming effect are two main challenges for realizing high-performance indoor OCC systems as shown in Fig. 10. Ground reflections and other illuminating light sources are two typical interferences. To cope with such negative influences, morphological operations which include dilation and erosion are first applied in our systems and the transmitter LED array can then be selected based on its imaging aspect ratio. Camera exposure time can be adjusted to avoid the blooming effect which is the solution we use in our system. Besides, the equalization technique and the appropriate selection of threshold are also of great help.

As a prototype indoor OCC system, an effective data rate (throughput) of 126.32 bps has been achieved which is suitable

TABLE V
OCC SYSTEMS PERFORMANCE ENHANCEMENT SOLUTIONS SUMMARY

Criteria	Objectives	Performance enhancement solutions		Ref.
Speed	Increase images per second	Improve camera frame rates		[69], [71]
		New camera types, i.e. event cameras		[24]
		Reduce processing area		[20], [69], [114], [115]
	Increase carrying bits per image	Improve LED numbers		[23], [24], [116], [117]
		RSE-based		[30]
		High-order modulations		[108], [113], [118], [119]
Distance	Power compensation	Increase transmitted power		[28]
		Increase camera gain		[78]
		Relay method		[111], [117]
	Enlarge LED imaging area	Increase camera focal length		[71]
		Apply camera defocus mode		[82]
		Spatial multiplexing based on coding		[97], [120], [121]
	Increase LED distinguishability	IPI alleviation		[71], [87], [123]
		Criteria modification		[40], [124]–[126]
Quality	Noise cancellation for channel	A neural network-based method		[127]
	Blur cancellation for image	Maximum likelihood-based detections		[128], [129]
		DL-based detections		[130]–[132]
		Increase frame rate to reduce motion blur		[28]
		Apply appropriate image compression scheme		[133]
	Avoid LED flickering perception	Dedicated modulations		[19], [20], [134]
		Coding, i.e., Manchester coding and AE		[135], [136]
Reliability	Angle distortion and blockage alleviation	RSE-based	PR, SSLD	[139]
			Grayscale redistribution	[140]
		Non-RSE-based	With a header frame	[141]
			With a hierarchical scheme	[142]
	Interference alleviation: Decrease blooming impact	Equalization and AI-based method		[143]–[148]
		Modify the applied threshold		[149]–[151]
	Interference alleviation: Decrease background impact	For RSE-based	ER, GVD, DNN	[152]–[154]
			Detach the background	[155]
		For non-RSE-based	Conventional methods	[156]
			Advanced methods	[130], [131], [157]
	Guarantee synchronization and avoid data dropout	Cameras with stable frame rates		[72]
		Repetitive schemes and spatial multiplexing		[97], [98]
		Packet estimation and reconstruction		[94], [158]
		Camera exposure time synchronization		[95]
	Link security	OCC location-aware ability		[159]
		Authentication protocol assisted by a verification key		[160]

TABLE VI
EXPERIMENTAL PARAMETERS FOR INDOOR USE EXAMPLE

Name of Parameter	Value of Parameter	Name of Parameter	Value of Parameter
LED layout	4 × 4 rectangular array	Camera image sensor	1/3" CCD
LED wavelength	808 nm	Camera shutter mode	GS
LED physical diameter	2 mm	Camera focal length	6 mm
LED driving current	75 mA	Camera resolution	720 (H)×576 (V)
LED irradiance angle	10°	Pixel size	4.75 μm × 4.75 μm
LED flickering rate	12 Hz	Camera frame rate	25 fps
LED array interval	3 cm	Camera exposure time	1×10^{-3} s

for indoor IoT-based data transmission. An error-free link up to 6 m and the maximum supported reliable link distance of 7.5 m (the achieved BER is below FEC threshold) has been realized based on the camera with a limited 6 mm focal length.

B. Outdoor OCC Experimental Platform Design Example

Our designed outdoor OCC platform serves as a prototype to test the technique's feasibility and practical performance for online outdoor scenarios. The transceiver is assumed to be parallel but can either be in static or mobile condition. The LED array is placed on a slide rail to realize mobility. The setup of the outdoor OCC platform is presented in Fig. 11.

1) System Main Parameters and Implementation: To further support high transmission distance, enhance the data rate, and guarantee the OCC system reliability for outdoor scenarios, a 4 × 4 LED array transmitter is extended to the scale of 8 × 8 based on the same LED type. A specially designed sCMOS-based

TABLE VII
EXPERIMENTAL PARAMETERS FOR OUTDOOR USE EXAMPLE

Name of Parameter	Value of Parameter	Name of Parameter	Value of Parameter
Camera focal length	11 mm-197 mm	Image capture card type	Dalsa OR-X4C0-XPF00
Camera resolution	2048 (H)×2048 (V)	Data interface	CameraLink
Camera pixel size	6.5 μm × 6.5 μm	Transmission bandwidth	1 Gbps
Maximum frame rate (with full resolution)	150 fps	Cache space	128 M

(a) (b) (c) (d)

Fig. 10. Demonstrations of indoor OCC systems design challenges. (a) Test environment. (b) Captured images with interference from reflections. (c) Captured images with interference from other light sources. (d) Captured images with blooming effect.

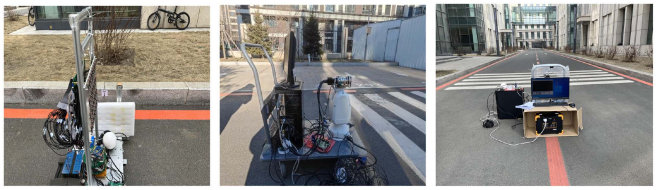

(a) (b) (c)

Fig. 11. The setup of the outdoor OCC platform. (a) The 808 nm 8 × 8 LED array. (b) The camera receiver. (c) The outdoor environment.

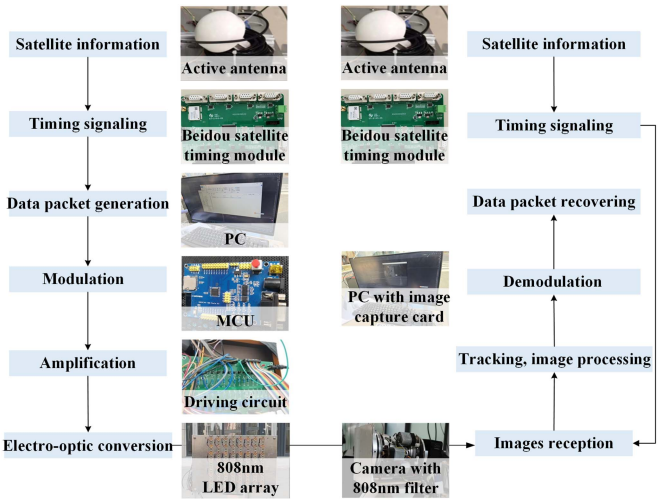

Fig. 12. Implementations of the outdoor OCC platform.

camera with an enhanced frame rate, variable focal length, and higher resolution is introduced for the outdoor OCC platform. An image capture card, which is inserted in the computer and connects the camera based on CameraLink, is applied to facilitate image transmission, storage, and further processing between the camera and the computer. Main parameter values of the sCMOS camera and the image capture card are presented in Table VII. Although the maximum camera frame rate is 150 fps (with full resolution), the applied camera frame rate is enhanced up to 200 fps based on the selected capture mechanism.

The implementation for outdoor scenarios is similar to the one for indoor environments except for the following aspects. The first difference is reflected in the driving circuit design at the transmitter side. Eight additional 74HC595 chips with I/O port expansion and serial-to-parallel conversion functionalities are used to realize 64 channels of data transmission due to the limited ports of the MCU and the large number of LEDs. Besides, four 74HC245 chips are used to further enhance the MCU driving ability. The second difference is reflected in the realization of synchronization. Apart from the frame synchronization based on SFH shown in Fig. 6, strict bit synchronization is realized based on the Beidou satellite timing module instead of the repetitive data transmission mechanism. Two Beidou satellite timing modules are applied at the transmitter and receiver side respectively, where their inside timing signals are synchronized based on the Beidou satellite. Such signals are used to control the data-sending time of the MCU and the image-capturing time of the camera. Based on such a synchronization mechanism, the LED flickering rate is possible to equal the camera frame rate without data dropout occurring. The third difference is that an image capture card substitutes the USB being applied to connect the camera with the processing computer to achieve higher data read rates. The camera-captured images are first written into the image capture card buffer, from which the computer reads pending images to realize further processing. As such cache space is limited, the applied image-based technique is required with high processing speed and low complexity to avoid image dropout caused by out-of-memory. Conventional template matching and projection methods are applied as LED tracking and detection methods respectively. Implementations of the outdoor OCC platform is presented in Fig. 12.

2) Design Challenges and Performance Achieved: Apart from interferences of the background and other light sources which are similar to indoor scenarios, attenuation of the LED distinguishability with the increase of the distance and motion-caused blur are two main challenges for realizing high-performance outdoor OCC systems. Loss of distinguishability can be seen obviously as shown in Fig. 13 when the distance increases from 20 m to 80 m, which then leads to image blur and power loss. These negative impacts may lead to a false location detection of the individual LED within an LED array and then further cause the bit error. Increasing the camera focal length and applying spatial multiplexing-based coding are two effective solutions. With the help of a variable-focal-length

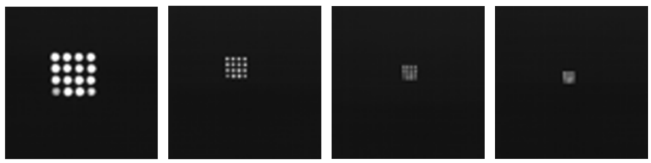

Fig. 13. Captured images under various distances. (a) 20 m. (b) 40 m. (c) 60 m. (d) 80 m.

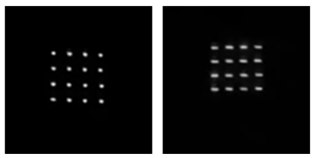

Fig. 14. Captured images under static and mobile conditions. (a) The static condition. (b) The mobile condition.

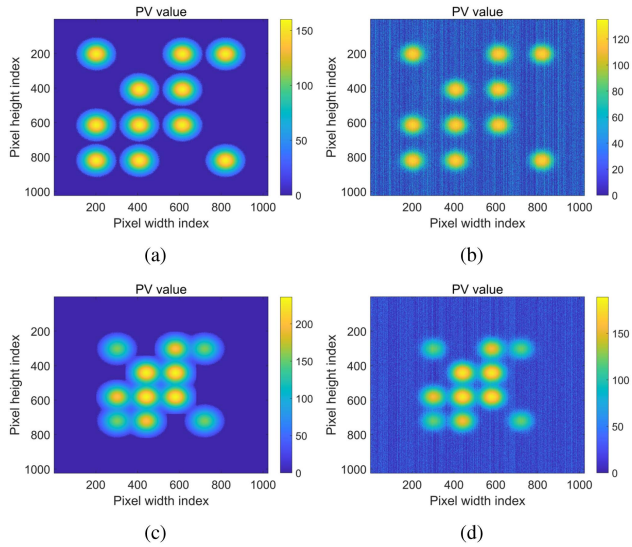

Fig. 15. (a) Non-overlapping MIMO-OCC simulated image for CCD camera. (b) Non-overlapping MIMO-OCC simulated image for CMOS camera. (c) Overlapping MIMO-OCC simulated image for CCD camera. (d) Overlapping MIMO-OCC simulated image for CMOS camera.

camera, individual LEDs can be captured clearly beyond 80 m on our OCC platform, leading to an extension of the transmission distance. Motion-caused blur is presented in Fig. 14, where the shape of the imaging LED has changed from a circular shape to an approximately elliptical shape. Simultaneously, angular distortion also occurs due to the movement of the LED transmitter. Such blur and deformation phenomena put great challenges on the design of shape-based LED detection methods. Higher frame rate cameras are recommended to compensate for the motion-induced blur, which is also the solution we take in our system. Besides, more advanced AI-based deblurring and posture correction algorithms can be considered.

For our outdoor OCC platform, a maximum data rate of 12.40 kbps is achieved based on testing results, and the longest supported distance is 80.09 m with the BER as 0.86×10^{-4}. The achieved performance can support outdoor-based OCC applications, such as location information broadcasting in V2V scenarios.

C. Simulated OCC System Design Example

Our simulated OCC system is presented to provide feasible details on simulation design principles. The purpose of our simulation is twofold, one is for analytical performance analysis, and the other is for the generation of synthetic OCC images for further processing.

1) Brief Descriptions of Simulation Procedures: The simulated OCC system is with the assumed Lambertian-pattern LED array-based transmitter, indoor optical channel, and camera receivers which include both CCD and CMOS types. Only GS mode is considered in our system. As transceivers are assumed to be parallel to each other without loss of generality, the simulated LED imaging areas appear in the centre of the images. (17) is first used to calculate the LED imaging radius. Then, (2) and (11) are applied to describe the transmitted optical power and channel path loss. The radiometric model which describes the camera's overall imaging process is used to calculate the corresponding pixel values. Both the realistic CCD and CMOS camera noises are considered in our simulations. Detailed analytical models and values of main parameters can be referred to in our published paper [28]. Two aspects of differences are reflected in this simulated OCC system: the individual LED-based OCC system is generalized to an LED array-based MIMO-OCC system, and the camera resolution is increased from 720 × 576 to 1024 × 1024.

2) Simulation Results and Related Analysis: The MIMO OCC simulated images for CCD and CMOS cameras considering their different internal noise characteristics are presented in Fig. 15. With the increase of transmission distance, the simulated LEDs in the array change from non-overlapping shown in Fig. 15(a), (b) to overlapping situations shown in Fig. 15(c), (d). Pixel values of the imaging area centre under the overlapping are also higher than those under the non-overlapping condition. Moreover, CCD cameras boast higher imaging quality than CMOS cameras which can be noticed obviously from Fig. 15 as well, where stripe-based camera noises can be seen in CMOS cameras clearly and their imaging pixel values are lower. In addition to the above qualitative analysis, quantitative data results based on D-PSNR and D-BER under various path loss coefficients γ are demonstrated in Fig. 16. Calculations of the PSNR and BER are based on (33) and (32) respectively. From Fig. 16, PSNR increases and BER decreases with the increase of D, and the larger the γ is, the more obvious the variation is ($\gamma \neq 2$). When path loss coefficient γ equals 2, both the PSNR and BER remain constant as the DC gain at a pixel remains stable based on (11).

D. Generalized Design Experience That can be Learned

Design experience learned from our OCC platforms is generalized to real-world applications in this part based on three design processes.

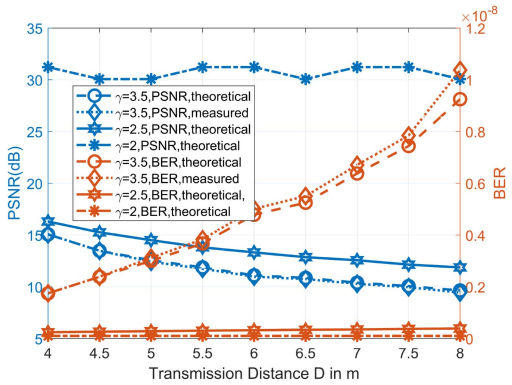

Fig. 16. D-PSNR and D-BER under various path loss coefficient γ.

Firstly, application scenarios and required system performance indicators should be clarified. Normally, for indoor scenarios such as the typical room office, restaurant, shopping mall or museum, the required distance is comparatively short (below 10 m or even centimeter level) while the supported data rate (up to kbps) and the transmission accuracy (below FEC threshold) are relatively high so that the location-based interactive services (indoor positioning, internet access, etc.) can be achieved. In contrast, for outdoor scenarios such as vehicular or drone-based communications, the designed system is expected to stand by long transmission distances (above 5 m) with good mobility support.

Secondly, system parameters and applied techniques should be carefully selected after identifying environmental characteristics and design challenges. For indoor OCC environments, as the supported distances are relatively limited, requirements for the physical size and transmitted optical power of LED transmitters, camera focal length and frame rate are relatively low. Off-the-shelf cameras and LEDs are able to fulfill basic communication necessities. Design challenges for indoor scenarios are mainly from the following aspects: interferences from the background and other light sources, blooming effect from adjacent transmitters, power loss and partial imaging due to angle distortion, and link blockage or even interruption. Besides, the supported distance, data rate, and link reliability are expected to increase. More advanced AI-based object detection algorithms can be integrated into OCC systems, and IoT-based indoor OCC applications, such as high-precise localization can be realized [163]. Power loss and the attenuation of the individual LED distinguishability are the two main factors leading to deteriorated outdoor-based OCC performance. The former is mainly due to the long transmission distance, angular distortion of the transceiver and weather impact. The latter is mostly due to the received blurry images caused by motion, foggy weather, and long transmission distance-induced high-frequency loss. Both the hardware selection and algorithm design can be considered to compensate for the above-mentioned disadvantages. For hardware modifications, transmitter LEDs with larger physical diameters and higher optical transmission power, and cameras with the improved focal length, frame rate, and resolutions are of great benefit but normally at a larger cost. For the algorithm design, accurate LED tracking and detection realizations can be achieved assisted by both the shape-based conventional methods such as template matching and Hough circle-based detection, and AI-based advanced methods such as Single Shot MultiBox Detector (SSD) and YOLO networks as long as the applied network structure and parameter are adjusted properly. Besides, the selected threshold for LED status judgement is also important in realizing high communication performance. As it's sensitive to distance, weather condition, and illumination intensity, threshold estimation can be made based on the training frame sequences ahead of the data transmission. Moreover, other OWC and RF-based technologies can also be considered to integrate with OCC in outdoor scenarios to further enhance the supported communication performance.

Finally, the system's overall cost and implementation complexity should be balanced. As OCC systems can be easily integrated with the fundamental infrastructure, provide no interference with the RF-based technology, and support abundant unlicensed spectrum, it's relatively easy to set up. Besides, as typical techniques required by a common OCC system including modulation/demodulation, coding/decoding, object tracking and detection are mature and relatively simple to achieve, the technical threshold of OCC is not high as well. In contrast to other OWC technologies such as FSO where high-powered laser transmitters and expensive pointing systems are in demand, the implementation complexity of OCC systems is comparatively low. To be more specific, we use our own designed system as an example. For our indoor OCC system which includes modulation and amplification part (<\$12), transmitter array with 16 LEDs (<\$7), camera receiver part (<\$28), and data processing part (<\$280), the hardware cost of the indoor experimental system is less than \$350. However, for practical application scenarios, indoor OCC systems can be easily integrated with the existing fixture lighting systems and a handheld smartphone is a good option for a receiver. It's cheaper and more convenient for large-scale deployments of indoor OCC based on the existing infrastructure with only the addition of modulation on the transmitter side and the image processing algorithm integrated into the receiver side. For our outdoor OCC system which includes modulation and amplification part (<\$12), transmitter array with 64 LEDs (<\$28), camera receiver part (<\$4200), and data processing part (<\$560), the hardware cost of the outdoor experimental system is less than \$4800. The sCMOS-based camera is the most expensive part of our outdoor OCC system and its data frame rate can achieve 150 fps under the resolution of 2048 $\times$ 2048 and can form clear images even in extreme weather conditions. We apply it for the sake of scientific research and design as a prototype to test the extreme performance it can achieve under our tested outdoor environment. However, for common outdoor scenarios such as vehicular communications, vehicle headlights and taillights can be used as transmitters and the dash cameras are enough to be used as receivers where the total system cost can be greatly decreased.

VII. Design Challenges and Future Research Directions

Five aspects of design challenges and their future research directions are introduced in this section which include accurate system modeling, physical layer optimization, AI-assisted OCC, security, and integration with other communication technologies.

A. Accurate System Modeling

System modeling plays a vital role in the theoretical analysis of OCC performance and is also fundamental for practical system design. How to accurately model OCC systems with more practical influential factors considered remains an open issue where the impact of the transceiver angular distortion and system asynchronous due to camera frame rate instability is expected to be integrated into future research. Besides, accurate NLOS and IRS-based OCC link modeling also remain to be investigated. Moreover, synthetic OCC images to support generations of a more accurate training data set for ML-based studies are envisaged to be achieved based on system modeling as well.

B. Physical Layer Techniques Optimization

Optimizations of physical layer techniques including synchronization, modulation, and error correction schemes are necessary for further enhancing future OCC systems. Most existing OCC systems use repetitive transmission schemes to alleviate the negative impact induced by loss of synchronization where the data transmission efficiency is lowered. Our applied satellite-based timing system can help to achieve accurate system synchronization but the hardware implementation is complicated. How to quickly realize OCC system synchronization based on the existing infrastructure and efficient algorithms is worthwhile to explore. An efficient modulation scheme design needs to consider the impact of the channel environment, illumination requirement, and eyes' comfort. Although the basic OOK is enough for most of the OCC prototype systems, investigating the adaptive modulation based on the above-mentioned requirements according to channel quality and system hardware performance is of great significance. Error correction is important in guaranteeing the system's reliability. Corrections based on repetitive transmission and applications of the error correction code are two existing common methods. Bidirectional OCC link where feedback indicating the transmission error, data fusion among multiple OCC transmitters, and multimodality-assisted DL networks are expected to further enhance OCC system error correction ability.

C. AI-Assisted OCC

AI has been proven to be a powerful tool in the OCC field where individual or multiple transmitters' tracking and detection, image deblurring, optical channel equalization, noise cancellation and dimming support are realized based on CNN, DNN, and GAN. In the future, on the one hand, more powerful network structures can be integrated into the OCC area where communication performance even under the existence of reflected light, weak lighting conditions, and obvious interferences can be guaranteed. On the other hand, other interesting functionalities such as DRL-based resource allocation and multimodality-assisted data fusion can be investigated.

D. Security

Most studies emphasize how to enhance the current optical link reliability while ignoring the legitimacy determination of the two communication parties. Scenarios such as eavesdropping and link attack are also lack of investigations. Security enhancement solutions such as location-aware-based identity authentication and key verification can be explored in the future.

E. Integration With Other Communication Technologies

As OCC can be integrated with the existing infrastructure and poses limited impact on the RF and OWC-based technologies, cooperation among OCC and other communication technologies can be realized to provide more strict guarantees on the practical scenarios' performance. Interesting research topics such as OCC/RF and OCC/OWC system deployment, handover algorithms design and resource allocation schemes can be studied.

VIII. Conclusion

Guidelines for OCC system design are presented in this paper from theory to practice. For OCC experimental platform design, suggestions for hardware parameter selection, overall system implementation procedures, evaluation criteria, performance enhancement solutions, and typical design examples are provided. For simulated OCC system design, analytical models of the transceiver and optical channel, simulated processes, and typical synthetic images with theoretical analysis are presented. This tutorial provides guidance for future OCC system design and potentially inspires further advances in OCC research development.

References

[1] S. R. Teli, P. Chvojka, S. Vitek, S. Zvanovec, R. Perez-Jimenez, and Z. Ghassemlooy, "A SIMO hybrid visible-light communication system for optical IoT," *IEEE Internet Things J.*, vol. 9, no. 5, pp. 3548–3558, Mar. 2022.

[2] P. Zhang et al., "Constraints and recent solutions of optical camera communication for practical applications," *Photonics*, vol. 10, no. 6, May 2023, Art. no. 608.

[3] M. Z. Chowdhury, M. Shahjalal, M. K. Hasan, and Y. M. Jang, "The role of optical wireless communication technologies in 5G/6G and IoT solutions: Prospects, directions, and challenges," *Appl. Sci.*, vol. 9, no. 20, Oct. 2019, Art. no. 4367.

[4] T. Nguyen, A. Islam, T. Hossan, and Y. M. Jang, "Current status and performance analysis of optical camera communication technologies for 5G networks," *IEEE Access*, vol. 5, pp. 4574–4594, 2017.

[5] N. Saeed, S. Guo, K.-H. Park, T. Y. Al-Naffouri, and M.-S. Alouini, "Optical camera communications: Survey, use cases, challenges, and future trends," *Phys. Commun.*, vol. 37, Dec. 2019, Art. no. 100900.

[6] W. A. Cahyadi, Y. H. Chung, Z. Ghassemlooy, and N. B. Hassan, "Optical camera communications: Principles, modulations, potential and challenges," *Electronics*, vol. 9, no. 9, Aug. 2020, Art. no. 1339.

[7] N. T. Le, M. A. Hossain, and Y. M. Jang, "A survey of design and implementation for optical camera communication," *Signal Process, Image Commun.*, vol. 53, pp. 95–109, Apr. 2017.

[8] W. Liu and Z. Xu, "Some practical constraints and solutions for optical camera communication," *Philos. Trans. Roy. Soc.*, vol. 378, Mar. 2020, Art. no. 2169.

[9] Z. Tang and T. Yamazato, "Image sensor communication and its transmitting devices," *Opt. Commun.*, vol. 541, Aug. 2023, Art. no. 129545.

[10] C.-W. Chow, "Recent advances and future perspectives in optical wireless communication, free space optical communication and sensing for 6G," *J. Lightw. Technol.*, vol. 42, no. 11, pp. 3972–3980, Jun. 2024.

[11] N. Saha, M. S. Ifthekhar, N. T. Le, and Y. M. Jang, "Survey on optical camera communications: Challenges and opportunities," *IET Optoelectron.*, vol. 9, no. 5, pp. 172–183, Oct. 2015.

[12] T. Nguyen, A. Islam, T. Yamazato, and Y. M. Jang, "Technical issues on IEEE 802.15.7 m image sensor communication standardization," *IEEE Commun. Mag.*, vol. 56, no. 2, pp. 213–218, Feb. 2018.

[13] N.-N. Dao, T.-H. Do, S. Cho, and S. Dustdar, "Information revealed by vision: A review on the next-generation OCC standard for AIoV," *IT Professional*, vol. 24, no. 4, pp. 58–65, Sep. 2022.

[14] H. Nguyen, I. B. K. Y. Utama, and Y. M. Jang, "Enabling technologies and new challenges in IEEE 802.15. 7 optical camera communications standard," *IEEE Commun. Mag.*, vol. 62, no. 3, pp. 90–95, Mar. 2024.

[15] IEEE Draft Standard for Local and Metropolitan Area Networks — Part 15.7: Short-Range Optical Wireless Communications Amendment: Higher Speed, Longer Range Optical Camera Communication (OCC), IEEE Standard P802.15.7a/D7, Jun. 2024.

[16] M. Shahjalal, M. K. Hasan, M. Z. Chowdhury, and Y. M. Jang, "Smartphone camera-based optical wireless communication system: Requirements and implementation challenges," *Electronics*, vol. 8, no. 8, Aug. 2019, Art. no. 913.

[17] M. Z. Chowdhury, M. T. Hossan, M. Shahjalal, M. K. Hasan, and Y. M. Jang, "A new 5G eHealth architecture based on optical camera communication: An overview, prospects, and applications," *IEEE Consum. Electron. Mag.*, vol. 9, no. 6, pp. 23–33, Nov. 2020.

[18] M. K. Hasan, M. O. Ali, M. H. Rahman, M. Z. Chowdhury, and Y. M. Jang, "Optical camera communication in vehicular applications: A review," *IEEE Trans. Intell. Transp. Syst.*, vol. 23, no. 7, pp. 6260–6281, Jul. 2022.

[19] P. Luo, M. Zhang, Z. Ghassemlooy, S. Zvanovec, S. Feng, and P. Zhang, "Undersampled-based modulation schemes for optical camera communications," *IEEE Commun. Mag.*, vol. 56, no. 2, pp. 204–212, Feb. 2018.

[20] T. L. Pham, M. Shahjalal, V. Bui, and Y. M. Jang, "Deep learning for optical vehicular communication," *IEEE Access*, vol. 8, pp. 102691–102708, 2020.

[21] S. Riurean, R. A. Dobre, and A.-E. Marcu, "Security and propagation issues and challenges in VLC and OCC systems," in *Proc. SPIE*, 2020, vol. 11718, pp. 580–585.

[22] K. Cui, G. Chen, Z. Xu, and R. D. Roberts, "Traffic light to vehicle visible light communication channel characterization," *Appl. Opt.*, vol. 51, no. 27, pp. 6594–6605, Sep. 2012.

[23] S. R. Teli, V. Matus, S. Zvanovec, R. Perez-Jimenez, S. Vitek, and Z. Ghassemlooy, "Optical camera communications for IoT–rolling-shutter based MIMO scheme with grouped LED array transmitter," *Sensors*, vol. 20, no. 12, Jun. 2020, Art. no. 3361.

[24] Z. Tang, T. Yamazato, and S. Arai, "A preliminary investigation for event camera-based visible light communication using the propeller-type rotary LED transmitter," in *Proc. IEEE Int. Conf. Commun. Workshops*, 2022, pp. 646–650.

[25] S. R. Teli, V. Matus, C. L. Aguiar, R. Perez-Jimenez, S. Zvanovec, and Z. Ghassemlooy, "Non line-of-sight optical camera communication employing a flexible OLED," in *Proc. IEEE South Amer. Conf. Visible Light Commun.*, 2023, pp. 1–5.

[26] A. D. Griffiths, J. Herrnsdorf, M. J. Strain, and M. D. Dawson, "Scalable visible light communications with a micro-LED array projector and high-speed smartphone camera," *Opt. Exp.*, vol. 27, no. 11, pp. 15585–15594, May 2019.

[27] T. Komine and M. Nakagawa, "Fundamental analysis for visible-light communication system using LED lights," *IEEE Trans. Consum. Electron.*, vol. 50, no. 1, pp. 100–107, Feb. 2004.

[28] A. Liu, W. Shi, M. Ouyang, and W. Liu, "Characterization of optical camera communication based on a comprehensive system model," *J. Lightw. Technol.*, vol. 40, no. 18, pp. 6087–6100, Sep. 2022.

[29] Q. Wang, P. Zhang, Y. Sun, and Y. Yang, "A general model for dimmable optical camera communication," in *Proc. Int. Conf. Sens., Meas. Data Anal. Era Artif. Intell.*, 2021, pp. 1–7.

[30] L. Zeng, D. O'Brien, H. Le-Minh, K. Lee, D. Jung, and Y. Oh, "Improvement of date rate by using equalization in an indoor visible light communication system," in *Proc. IEEE Int. Conf. Circuits Syst. Commun.*, 2008, pp. 678–682.

[31] Z. Ghassemlooy, D. Wu, M.-A. Khalighi, and X. Tang, "Indoor non-directed optical wireless communications optimization of the lambertian order," *J. Elect. Comput. Eng. Innovations*, vol. 1, no. 1, pp. 1–10, May 2013.

[32] P. Luo, Z. Ghassemlooy, H. Le Minh, E. Bentley, A. Burton, and X. Tang, "Performance analysis of a car-to-car visible light communication system," *Appl. Opt.*, vol. 54, no. 7, pp. 1696–1706, Mar. 2015.

[33] T.-H. Do and M. Yoo, "Performance analysis of visible light communication using CMOS sensors," *Sensors*, vol. 16, no. 3, Feb. 2016, Art. no. 309.

[34] A. Burton, Z. Ghassemlooy, S. Rajbhandari, and S.-K. Liaw, "Design and analysis of an angular-segmented full-mobility visible light communications receiver," *Trans. Emerg. Telecommun. Technol.*, vol. 25, no. 6, pp. 591–599, Mar. 2014.

[35] A. Singh, A. Srivastava, V. A. Bohara, and G. S. V. R. K. Rao, "Performance of indoor visible light communication system under random placement of LEDs," in *Proc. IEEE 21st Int. Conf. Transp. Opt. Netw.*, 2019, pp. 1–5.

[36] A. Burton, H. Le Minh, Z. Ghasemlooy, and S. Rajbhandari, "A study of LED lumination uniformity with mobility for visible light communications," in *Proc. IEEE Int. Workshop Opt. Wireless Commun.*, 2012, pp. 1–3.

[37] T.-H. Do and M. Yoo, "The necessity of LED to ambient light ratio optimization for vehicular optical camera communication," *Sensors*, vol. 20, no. 1, Jan. 2020, Art. no. 292.

[38] B. Nurfadhilah, B. Pamukti, and D. M. Saputri, "Performance of LED overlap in visible light communication system," in *Proc. IEEE Asia Pacific Conf. Wireless Mobile*, Bali, Indonesia, Jan. 2019, pp. 42–47.

[39] W. Guan, Y. Wu, C. Xie, L. Fang, X. Liu, and Y. Chen, "Performance analysis and enhancement for visible light communication using CMOS sensors," *Opt. Commun.*, vol. 410, pp. 531–551, Mar. 2018.

[40] T.-H. Do and M. Yoo, "A multi-feature LED bit detection algorithm in vehicular optical camera communication," *IEEE Access*, vol. 7, pp. 95797–95811, 2019.

[41] P. Liu, P. Zheng, S. Yang, and Z. Chen, "Modeling and analysis of spatial inter-symbol interference for RGB image sensors based on visible light communication," *Sensors*, vol. 19, no. 22, Nov. 2019, Art. no. 4999.

[42] A. Memedi, H.-M. Tsai, and F. Dressler, "Impact of realistic light radiation pattern on vehicular visible light communication," in *Proc. IEEE Glob. Commun. Conf.*, 2017, pp. 1–6.

[43] W. Viriyasitavat, S.-H. Yu, and H.-M. Tsai, "Short paper: Channel model for visible light communications using off-the-shelf scooter taillight," in *Proc. IEEE. Veh. Netw. Conf.*, 2013, pp. 170–173.

[44] X. Zhang, G. Klevering, K. Wijewardena, and L. Xiao, "Integrated on-site localization and optical camera communication for drones," in *Proc. IEEE 24th Int. Symp. World Wireless, Mobile, Multimedia Netw.*, 2023, pp. 334–336.

[45] Y.-H. Chang et al., "Water-to-air PAM4 optical camera communication using long short term memory neural network (LSTM-NN)," in *Proc. Opt. Fiber Commun. Conf. Exhib.*, 2024, pp. 1–3.

[46] B. Majlesein, C. T. Geldard, V. Guerra, J. Rufo, W. O. Popoola, and J. Rabadan, "Empirical study of an underwater optical camera communication system under turbulent conditions," *Opt. Exp.*, vol. 31, no. 13, pp. 21493–21506, Jun. 2023.

[47] S. Yahia, Y. Meraihi, A. Ramdane-Cherif, A. B. Gabis, D. Acheli, and H. Guan, "A survey of channel modeling techniques for visible light communications," *J. Netw. Comput. Appl.*, vol. 194, Sep. 2021, Art. no. 103206.

[48] B. Turan, G. Gurbilek, A. Uyrus, and S. C. Ergen, "Vehicular VLC frequency domain channel sounding and characterization," in *Proc. IEEE Veh. Netw. Conf.*, 2018, pp. 1–8.

[49] J. M. Kahn and J. R. Barry, "Wireless infrared communications," *Proc. IEEE*, vol. 85, no. 2, pp. 265–298, Feb. 1997.

[50] B. Turan and S. Coleri, "Machine learning based channel modeling for vehicular visible light communication," *IEEE Trans. Veh. Technol.*, vol. 70, no. 10, pp. 9659–9672, Oct. 2021.

[51] K. Cui, G. Chen, Z. Xu, and R. D. Roberts, "Line-of-sight visible light communication system design and demonstration," in *Proc. 7th Int. Symp. Commun. Syst., Netw. Digit. Signal Process.*, Jul., 2010, pp. 621–625.

[52] M. Elamassie, M. Karbalayghareh, F. Miramirkhani, R. C. Kizilirmak, and M. Uysal, "Effect of fog and rain on the performance of vehicular visible light communications," in *Proc. IEEE 87th Veh. Technol. Conf.*, 2018, pp. 1–6.

[53] H. B. Eldeeb, F. Miramirkhani, and M. Uysal, "A path loss model for vehicle-to-vehicle visible light communications," in *Proc. IEEE 15th Int. Conf. Telecommun.*, 2019, pp. 1–5.

[54] J. Ding, Z. Xu, and L. Hanzo, "Accuracy of the point-source model of a multi-LED array in high-speed visible light communication channel characterization," *IEEE Photon. J.*, vol. 7, no. 4, Aug. 2015, Art. no. 1600714.

[55] F. Miramirkhani, O. Narmanlioglu, M. Uysal, and E. Panayirci, "A mobile channel model for VLC and application to adaptive system design," *IEEE Commun. Lett.*, vol. 21, no. 5, pp. 1035–1038, May 2017.

[56] F. Miramirkhani and M. Uysal, "Channel modeling and characterization for visible light communications," *IEEE Photon. J.*, vol. 7, no. 6, Dec. 2015, Art. no. 7905616.

[57] J. Chen and C. Yan, "A channel model for indoor visible light communication system with specular reflection," in *Proc. IEEE 16th Int. Conf. Opt. Commun. Netw.*, 2017, pp. 1–3.

[58] A. Kumar and V. Sudha, "Optical power distribution and statistical analysis of indoor visible light communication," in *Proc. IEEE TEQIP III Sponsored Int. Conf. Microw. Integr. Circuits, Photon. Wireless Netw.*, 2019, pp. 383–386.

[59] R. Raj, S. Jaiswal, and A. Dixit, "On the effect of multipath reflections in indoor visible light communication links: Channel characterization and BER analysis," *IEEE Access*, vol. 8, pp. 190620–190636, 2020.

[60] A.-L. Chen, H.-P. Wu, Y.-L. Wei, and H.-M. Tsai, "Time variation in vehicle-to-vehicle visible light communication channels," in *Proc. IEEE Veh. Netw. Conf.*, 2016, pp. 1–8.

[61] T. Yamazato et al., "Vehicle motion and pixel illumination modeling for image sensor based visible light communication," *IEEE J. Sel. Areas Commun.*, vol. 33, no. 9, pp. 1793–1805, Sep. 2015.

[62] S. Lee, J. K. Kwon, S.-Y. Jung, and Y.-H. Kwon, "Evaluation of visible light communication channel delay profiles for automotive applications," *EURASIP J. Wireless Commun. Netw.*, vol. 2012, no. 1, pp. 370:1–370:8, Dec. 2012.

[63] M. A. Atta and A. Bermak, "Channel length modeling for a multiple-input-multiple-output camcom link," in *Proc. IEEE Int. Conf. Adv. Wireless Opt. Commun.*, 2018 pp. 78–82.

[64] L.-C. Wu and H.-M. Tsai, "Modeling vehicle-to-vehicle visible light communication link duration with empirical data," in *Proc. IEEE Globecom Workshops*, 2013, pp. 1103–1109.

[65] V. Matus, E. Eso, S. R. Teli, R. Perez-Jimenez, and S. Zvanovec, "Experimentally derived feasibility of optical camera communications under turbulence and fog conditions," *Sensors*, vol. 20, no. 3, Jan. 2020, Art. no. 757.

[66] V. Georlette, S. Bette, S. Brohez, R. Pérez-Jiménez, N. Point, and V. Moeyaert, "Outdoor visible light communication channel modeling under smoke conditions and analogy with fog conditions," *Optics*, vol. 1, no. 3, pp. 259–281, Nov. 2020.

[67] V. Matus, V. Guerra, S. Zvanovec, J. Rabadan, and R. Perez-Jimenez, "Sandstorm effect on experimental optical camera communication," *Appl. Opt.*, vol. 60, no. 1, pp. 75–82, Dec. 2021.

[68] D. Moreno, J. Rufo, V. Guerra, J. Rabadan, and R. Perez-Jimenez, "Effect of temperature on channel compensation in optical camera communication," *Electronics*, vol. 10, no. 3, Jan. 2021, Art. no. 262.

[69] I. Takai, T. Harada, M. Andoh, K. Yasutomi, K. Kagawa, and S. Kawahito, "Optical vehicle-to-vehicle communication system using LED transmitter and camera receiver," *IEEE Photon. J.*, vol. 6, no. 5, Oct. 2014, Art. no. 7902513.

[70] D. Moreno, V. Guerra, J. Rufo, J. Rabadan, and R. Perez-Jimenez, "Multispectral optical camera communication links based on spectral signature multiplexing," *IET Optoelectron.*, vol. 17, no. 4, pp. 91–100, Jun. 2023.

[71] T. Kasashima, T. Yamazato, H. Okada, T. Fujii, T. Yendo, and S. Arai, "Interpixel interference cancellation method for road-to-vehicle visible light communication," in *Proc. IEEE 5th Int. Symp. Wireless Veh. Commun.*, 2013, pp. 1–5.

[72] P. Nguyen, N. T. Le, and Y. M. Jang, "Challenges issues for OCC based android camera 2 API," in *Proc. IEEE 9th Int. Conf. Ubiquitous Future Netw.*, 2017, pp. 669–673.

[73] G. Simon and M. Rátosi, "Characterization and measurement of performance properties of the UFSOOK camera communication protocol," *IEEE Trans. Instrum. Meas.*, vol. 69, no. 10, pp. 7982–7989, Oct. 2020.

[74] M. Sugimoto, H. Kumaki, T. Akiyama, and H. Hashizume, "Optimally modulated illumination for rapid and accurate time synchronization," *IEEE Trans. Signal Process.*, vol. 65, no. 2, pp. 505–516, Jan. 2017.

[75] S. Vitek, J. Libich, P. Luo, S. Zvanovec, Z. Ghassemlooy, and N. B. Hassan, "Influence of camera setting on vehicle-to-vehicle VLC employing undersampled phase shift on-off keying," *Radioengineering*, vol. 26, no. 4, pp. 946–953, Aug. 2017.

[76] S. R. Teli, S. Zvanovec, and Z. Ghassemlooy, "The first tests of smartphone camera exposure effect on optical camera communication links," in *Proc. IEEE 15th Int. Conf. Telecommun.*, 2019, pp. 1–6.

[77] M. K. Hasan, M. Z. Chowdhury, M. Shahjalal, V. T. Nguyen, and Y. M. Jang, "Performance analysis and improvement of optical camera communication," *Appl. Sci.*, vol. 8, no. 12, Dec. 2018, Art. no. 2527.

[78] V. Matus et al., "Experimental evaluation of an analog gain optimization algorithm in optical camera communications," in *Proc. IEEE 12th Int. Symp. Commun. Syst. Netw. Digit. Signal Process*, 2020, pp. 1–5.

[79] N. B. Hassan et al., "Impact of camera lens aperture and the light source size on optical camera communications," in *Proc. IEEE 11th Int. Symp. Commun. Syst. Netw. Digit. Signal Process.*, 2018, pp. 1–5.

[80] M. Konnik and J. Welsh, "High-level numerical simulations of noise in CCD and CMOS photosensors: Review and tutorial," 2014, *arXiv:1412.4031*.

[81] W. Huang and Z. Xu, "Characteristics and performance of image sensor communication," *IEEE Photon. J.*, vol. 9, no. 2, Apr. 2017, Art. no. 7902919.

[82] E. Eso, S. Teli, N. B. Hassan, S. Vitek, Z. Ghassemlooy, and S. Zvanovec, "400 m rolling-shutter-based optical camera communications link," *Opt. Lett.*, vol. 45, no. 5, pp. 1059–1062, Feb. 2020.

[83] M. Seminara, T. Nawaz, S. Caputo, L. Mucchi, and J. Catani, "Characterization of field of view in visible light communication systems for intelligent transportation systems," *IEEE Photon. J.*, vol. 12, no. 4, Aug. 2020, Art. no. 7903816.

[84] N. M. Esfahani, A. Gholami, N. S. Kordavani, S. Zvanovec, and Z. Ghassemlooy, "The impact of camera parameters on the performance of V2V optical camera communications," in *Proc. IEEE 12th Int. Symp. Commun. Syst. Netw. Digit. Signal Process.*, 2020, pp. 1–4.

[85] K. Dong, X. Ke, X. Zhang, and M. Wang, "Parametric modeling and experimental measurement of rolling shutter characteristics for optical camera communication using undersampled modulation," *Appl. Opt.*, vol. 61, no. 27, pp. 7838–7845, Sep. 2022.

[86] M. S. Ifthekhar, M. A. Hossain, C. H. Hong, and Y. M. Jang, "Radiometric and geometric camera model for optical camera communications," in *Proc. IEEE 7th Int. Conf. Ubiquitous Future Netw.*, 2015, pp. 53–57.

[87] P. Chavez-Burbano, V. Guerra, J. Rabadan, D. Rodríguez-Esparragón, and R. Perez-Jimenez, "Experimental characterization of close-emitter interference in an optical camera communication system," *Sensors*, vol. 17, no. 7, Jul. 2017, Art. no. 1561.

[88] J. C. Chau and T. D. Little, "Analysis of CMOS active pixel sensors as linear shift-invariant receivers," in *Proc. IEEE. Int. Conf. Commun. Workshop*, 2015, pp. 1398–1403.

[89] X. Li, N. B. Hassan, A. Burton, Z. Ghassemlooy, S. Zvanovec, and R. Perez-Jimenez, "A simplified model for the rolling shutter based camera in optical camera communications," in *Proc. 15th Int. Conf. Telecommun.*, 2019, pp. 1–5.

[90] G. Cossu, A. Sturniolo, and E. Ciaramella, "Modelization and characterization of a CMOS camera as an optical real-time oscilloscope," *IEEE Photon. J.*, vol. 12, no. 6, Dec. 2020, Art. no. 7906313.

[91] C. Jurado-Verdu, V. Guerra, V. Matus, J. Rabadan, and R. Perez-Jimenez, "Convolutional autoencoder for exposure effects equalization and noise mitigation in optical camera communication," *Opt. Exp.*, vol. 29, no. 15, pp. 22973–22991, Jul. 2021.

[92] J. Perez-Ramirez and D. K. Borah, "A single-input multiple-output optical system for mobile communication: Modeling and validation," *IEEE Photon. Tech. Lett.*, vol. 26, no. 4, pp. 368–371, Feb. 2014.

[93] H. Zhang and F. Yang, "Push the limit of light-to-camera communication," *IEEE Access*, vol. 8, pp. 55969–55979, 2020.

[94] X. Li, W. Liu, and Z. Xu, "Design and implementation of a rolling shutter based image sensor communication system," in *Proc. IEEE/CIC Int. Conf. Commun. China*, 2020, pp. 253–258.

[95] H. Matsunaga, T. Yendo, S. Arai, and T. Yamazato, "Exposure synchronization in optical camera communications for time division multiplexing," *IEEE Photon. J.*, vol. 15, no. 2, Apr. 2023, Art. no. 7301315.

[96] R. D. Roberts, "Undersampled frequency shift ON-OFF keying (UFSOOK) for camera communications (CamCom)," in *Proc. 22nd Wireless Opt. Commun. Conf.*, 2013, pp. 645–648.

[97] S. Arai et al., "Experimental on hierarchical transmission scheme for visible light communication using LED traffic light and high-speed camera," in *Proc. IEEE 66th Veh. Technol. Conf.*, 2007, pp. 2174–2178.

[98] H. Wu et al., "OnionCode: Enabling multi-priority coding in LED-based optical camera communications," in *Proc. IEEE Conf. Comput. Commun.*, 2022, pp. 260–269.

[99] A. Duque, R. Stanica, H. Rivano, and A. Desportes, "Analytical and simulation tools for optical camera communications," *Comput. Commun.*, vol. 160, pp. 52–62, Jul. 2020.

[100] N. M. Tuan, T. V. Phuong, T.-H. Do, and N. T. V. Khanh, "An highly realistic optical camera communication simulation framework for Internet of Things applications," in *Proc. IEEE 21st ACIS Int. Winter Conf. Softw. Eng., Artif. Intell., Netw. Parallel/Distrib. Comput.*, 2021, pp. 240–242.

[101] V. Matus, V. Guerra, C. Jurado-Verdu, J. Rabadán, and R. Perez-Jimenez, "Simulation of rolling shutter acquisition in optical camera communications," in *Proc. IEEE 15th Int. Conf. Telecommun.*, 2019, pp. 1–5.

[102] S. Salvi and V. Geetha, "A nested texture inspired novel image pattern based optical camera communication," *IEEE Access*, vol. 10, pp. 109056–109067, 2022.

[103] L. R. Ximenes and M. F. Alves, "Tensor-based screen-to-camera communications," *IEEE Commun. Lett.*, vol. 27, no. 10, pp. 2787–2791, Oct. 2023.

[104] S. Chen and X. Chi, "Analysis of optical camera communications for terminal jiggle with quality of service guarantees," *J. Lightw. Technol.*, vol. 41, no. 19, pp. 6280–6287, Oct. 2023.

[105] Z. Wang, J. Han, J. Liang, and L. Zhang, "Joint interframe separation and gamma correction for asynchronous optical camera communication systems based on high-order statistics," *Opt. Exp.*, vol. 32, no. 8, pp. 14808–14825, Apr. 2024.

[106] A. Liu, W. Shi, M. Safari, and W. Liu, "Investigating the angular distortion impact on vehicular optical camera communication (OCC) systems," *Opt. Exp.*, vol. 32, no. 11, pp. 19697–19715, May 2024.

[107] M. Eghbal, F. S. Tabataba, A. Gholami, J. Abouei, and M. Uysal, "Effect of a vehicle's mobility on SNR and SINR in vehicular optical camera communication systems," *Opt. Exp.*, vol. 32, no. 7, pp. 12257–12275, Mar. 2024.

[108] Y. Yang, J. Hao, and J. Luo, "CeilingTalk: Lightweight indoor broadcast through LED-camera communication," *IEEE Trans. Mobile Comput.*, vol. 16, no. 12, pp. 3308–3319, Dec. 2017.

[109] A. Ashok, S. Jain, M. Gruteser, N. Mandayam, W. Yuan, and K. Dana, "Capacity of screen–camera communications under perspective distortions," *Pervasive Mobile Comput.*, vol. 16, pp. 239–250, Jan. 2015.

[110] A. Islam, L. Musavian, and N. Thomos, "Performance analysis of vehicular optical camera communications: Roadmap to uRLLC," in *Proc. IEEE Glob. Commun. Conf.*, 2019, pp. 1–6.

[111] M. K. Hasan, M. Z. Chowdhury, M. Shahjalal, M. M. Islam, and Y. M. Jang, "Optimum LED coverage utilization in OCC for effective communication with mobile robot," *J. Commun. Netw.*, vol. 22, no. 5, pp. 371–379, Oct. 2020.

[112] R. D. Roberts, "Intel proposal in IEEE 802.15.7r1," Accessed on: Aug. 2016. [Online]. Available: https://mentor.ieee.org/802.15/dcn/16/15-16-0006-01-007a-intel-occ-proposal.pdf

[113] K. Dong, X. Ke, and H. Li, "Camera-based channel modeling and symbol error rate analysis of CSK modulation for outdoor OCC systems," *IEEE Access*, vol. 10, pp. 50254–50264, 2022.

[114] S. Teli, W. A. Cahyadi, and Y. H. Chung, "High-speed optical camera V2V communications using selective capture," *Photon. Netw. Commun.*, vol. 36, no. 2, pp. 210–216, Jun. 2018.

[115] M. R. A. Nasution, H. Herfandi, O. S. Sitanggang, H. Nguyen, and Y. M. Jang, "Proximity-based optical camera communication with multiple transmitters using deep learning," *Sensors*, vol. 24, no. 2, Jan. 2024, Art. no. 702.

[116] W. J. Ryu and S. Y. Shin, "RGB MIMO optical camera communication with histogram equalization," in *Proc. IEEE Int. Conf. Signals Syst.*, 2017, pp. 303–307.

[117] H. Takano, M. Nakahara, K. Suzuoki, Y. Nakayama, and D. Hisano, "300-meter long-range optical camera communication on RGB-LED-equipped drone and object-detecting camera," *IEEE Access*, vol. 10, pp. 55073–55080, 2022.

[118] J. He and Y. Yang, "Artificial neural network-based scheme for 4-PWM OCC system," *IEEE Photon. Technol. Lett.*, vol. 34, no. 6, pp. 333–336, Mar. 2022.

[119] Q. Chen et al., "Spaced color shift keying modulation for camera-based visible light communication system using rolling shutter effect," *Opt. Commun.*, vol. 449, pp. 19–23, Oct. 2019.

[120] Y. Amano, K. Kamakura, and T. Yamazato, "Alamouti-type coding for visible light communication based on direct detection using image sensor," in *Proc. IEEE Glob. Commun. Conf.*, 2013, pp. 2430–2435.

[121] K. Ebihara, K. Kamakura, and T. Yamazato, "Layered space-time coding using LED array for image-sensor-based visible light communications," in *Proc. IEEE Int. Conf. Commun.*, 2015, pp. 5048–5053.

[122] D. Vuong and M. Yoo, "Interpixel interference mitigation in visible light communication using image sensor," *IEEE Access*, vol. 6, pp. 45543–45551, 2018.

[123] R. Wu, Y. Guo, J. Liu, and P. Liu, "Modeling and analysis of spatial inter-symbol interference for MIMO image sensors based visible light communication," in *Proc. IEEE ITU Kaleidoscope: Challenges Data-Driven Soc.*, 2017, pp. 1–7.

[124] S. Wang, J. Liu, X. Zheng, A. Yang, Y. Song, and X. Guo, "Non-threshold demodulation algorithm for CMOS camera-based visible light communication," in *Proc. IEEE Opto-Electron. Commun. Conf.*, 2020, pp. 1–3.

[125] T.-H. Do and M. Yoo, "An image gradient based LED bit detection algorithm in vehicular optical camera communication," in *Proc. 11th Int. Conf. Ubiquitous Future Netw.*, 2019, pp. 617–619.

[126] Y. Xiao, W. Guan, S. Wen, J. Li, Z. Li, and M. Liu, "The optical bar code detection method based on optical camera communication using discrete fourier transform," *IEEE Access*, vol. 8, pp. 123238–123252, 2020.

[127] T. L. Pham, H. Nguyen, T. Nguyen, and Y. M. Jang, "A novel neural network-based method for decoding and detecting of the DS8-PSK scheme in an OCC system," *Appl. Sci.*, vol. 9, no. 11, May 2019, Art. no. 2242.

[128] Y. Ohira, T. Yendo, and S. Arai, "Development of low-complexity MLE method for image-sensor-based visible light communication," in *Proc. IEEE Veh. Netw. Conf.*, 2016, pp. 1–4.

[129] S. Arai, H. Matsushita, Y. Ohira, T. Yendo, D. He, and T. Yamazato, "Maximum likelihood decoding based on pseudo-captured image templates for image sensor communication," *Nonlinear Theory Appl., IEICE*, vol. 10, no. 2, pp. 173–189, Apr. 2019.

[130] A. Islam, M. T. Hossan, and Y. M. Jang, "Convolutional neural networkscheme–based optical camera communication system for Intelligent Internet of Vehicles," *Int. J. Distrib. Sens. Netw.*, vol. 14, no. 4, 2018, Art. no. 1550147718770153.

[131] X. Sun, W. Shi, Q. Cheng, W. Liu, Z. Wang, and J. Zhang, "An LED detection and recognition method based on deep learning in vehicle optical camera communication," *IEEE Access*, vol. 9, pp. 80897–80905, 2021.

[132] M. F. Ahmed, N. Pervin, S. Bhowmik, M. A. Rashid, A. Kuwana, and H. Kobayashi, "Design and implementation of remote controlling system using GAN in optical camera communication," *IEEE Photon. J.*, vol. 15, no. 2, Apr. 2023, Art. no. 7301510.

[133] X. Zhu, J. Chen, Z. He, A. Cai, and C. Yu, "Effect of an image compression scheme on optical camera communication," *Appl. Opt.*, vol. 63, no. 17, pp. 4713–4721, Jun. 2024.

[134] P. Luo, Z. Ghassemlooy, H. Le Minh, X. Tang, and H.-M. Tsai, "Undersampled phase shift ON-OFF keying for camera communication," in *Proc. 6th Int. Conf. Wireless Commun. Signal Process.*, 2014, pp. 1–6.

[135] H. Lee, I. Lee, T. Q. Quek, and S. H. Lee, "Binary signaling design for visible light communication: A deep learning framework," *Opt. Exp.*, vol. 26, no. 14, pp. 18131–18142, Jun. 2018.

[136] C. Zou and F. Yang, "Dimming-aware deep learning approach for OOK-based visible light communication," *J. Lightw. Technol.*, vol. 38, no. 20, pp. 5733–5742, Oct. 2020.

[137] Y. Wang, B. Hussain, and C. P. Yue, "Arbitrarily tilted receiver camera correction and partially blocked led image compensation for indoor visible light positioning," *IEEE Sens. J.*, vol. 22, no. 6, pp. 4800–4807, Mar. 2022.

[138] T.-H. Do and M. Yoo, "Multiple exposure coding for short and long dual transmission in vehicle optical camera communication," *IEEE Access*, vol. 7, pp. 35148–35161, 2019.

[139] K. Jiang, X. Chi, F. Ji, and S. Li, "Research on mobile phone swaying and receiving position in optical camera communication," *Optoelectron. Lett.*, vol. 18, no. 2, pp. 85–90, Feb. 2022.

[140] C.-W. Chow, Z.-Q. Li, Y.-C. Chuang, X.-L. Liao, K.-H. Lin, and Y.-Y. Chen, "Decoding CMOS rolling-shutter pattern in translational or rotational motions for VLC," *IEEE Photon. J.*, vol. 11, no. 2, Apr. 2019, Art. no. 7902305.

[141] W. A. Cahyadi, Y. H. Kim, Y. H. Chung, and C.-J. Ahn, "Mobile phone camera-based indoor visible light communications with rotation compensation," *IEEE Photon. J.*, vol. 8, no. 2, Apr. 2016, Art. no. 7903308.

[142] S.-H. Chen and C.-W. Chow, "Hierarchical scheme for detecting the rotating MIMO transmission of the in-door RGB-LED visible light wireless communications using mobile-phone camera," *Opt. Commun.*, vol. 335, pp. 189–193, Jan. 2015.

[143] L. Liu, R. Deng, and L.-K. Chen, "Spatial and time dispersions compensation with double-equalization for optical camera communications," *IEEE Photon. Technol. Lett.*, vol. 31, no. 21, pp. 1753–1756, Nov. 2019.

[144] L. Liu, R. Deng, and L.-K. Chen, "47-kbit/s RGB-LED-based optical camera communication based on 2D-CNN and XOR-based data loss compensation," *Opt. Exp.*, vol. 27, no. 23, pp. 33840–33846, Nov. 2019.

[145] K.-L. Hsu et al., "Rolling-shutter-effect camera-based visible light communication using RGB channel separation and an artificial neural network," *Opt. Exp.*, vol. 28, no. 26, pp. 39956–39962, Dec. 2020.

[146] D.-C. Tsai et al., "Using pixel-per-bit neural network for two rolling shutter patterns decoding in optical camera communication (OCC)," in *Proc. IEEE 30th Wireless Opt. Commun. Conf.*, 2021, pp. 102–105.

[147] Y. Noma, K. Murakami, T. Kato, and W. Chujo, "Increasing symbol rate by ensemble averaging with dual camera in rolling-shutter optical camera communication," *IEICE Commun. Exp.*, vol. 9, no. 7, pp. 300–305, Apr. 2020.

[148] M. Kinoshita, T. Toguma, S. Yamaguchi, S. Ibaraki, K. Kamakura, and T. Yamazato, "Performance enhancement of rolling shutter based visible light communication via selective reception using dual cameras," in *Proc. IEEE 19th Annu. Consum. Commun. Netw. Conf.*, 2022, pp. 853–857.

[149] W.-C. Wang, C.-W. Chow, L.-Y. Wei, Y. Liu, and C.-H. Yeh, "Long distance non-line-of-sight (NLOS) visible light signal detection based on rolling-shutter-patterning of mobile-phone camera," *Opt. Exp.*, vol. 25, no. 9, pp. 10103–10108, Apr. 2017.

[150] K. Liang, C.-W. Chow, Y. Liu, and C.-H. Yeh, "Thresholding schemes for visible light communications with CMOS camera using entropy-based algorithms," *Opt. Exp.*, vol. 24, no. 22, pp. 25641–25646, Oct. 2016.

[151] C.-W. Chen, C.-W. Chow, Y. Liu, and C.-H. Yeh, "Efficient demodulation scheme for rolling-shutter-patterning of CMOS image sensor based visible light communications," *Opt. Exp.*, vol. 25, no. 20, pp. 24362–24367, Sep. 2017.

[152] C.-W. Chow et al., "Secure mobile-phone based visible light communications with different noise-ratio light-panel," *IEEE Photon. J.*, vol. 10, no. 2, Apr. 2018, Art. no. 7902806.

[153] K.-L. Hsu et al., "CMOS camera based visible light communication (VLC) using grayscale value distribution and machine learning algorithm," *Opt. Exp.*, vol. 28, no. 2, pp. 2427–2432, Jan. 2020.

[154] R. Xiao, L. Zhao, F. Qian, L. Yang, and J. Han, "Practical optical camera communication behind unseen and complex backgrounds," in *Proc. 22nd Annu. Int. Conf. Mobile Syst., Appl. Serv.*, 2024, pp. 113–126.

[155] Z. Liu et al., "CORE-lens: Simultaneous communication and object REcognition with disentangled-GAN cameras," in *Proc. ACM 28th Annu. Int. Conf. Mobile Comput. Netw.*, 2022, pp. 172–185.

[156] P. Liu, X. Chen, Y. Li, and J. Liu, "A quick algorithm to detect LED array from the background in image sensor based visible light communication," in *Proc. IEEE Int. Conf. Imag. Syst. Techn.*, 2018, pp. 1–5.

[157] I. B. K. Y. Utama, O. S. Sitanggang, M. R. A. Nasution, M. I. Joha, J. Yoo, and Y. M. Jang, "Enhancing optical camera communication performance for collaborative communication using positioning information," *IEEE Access*, vol. 12, pp. 11795–11809, 2024.

[158] J. He, Y. Zhou, R. Deng, J. Shi, Z. Jiang, and Q. Tang, "Efficient sampling scheme based on length estimation for optical camera communication," *IEEE Photon. Technol. Lett.*, vol. 31, no. 11, pp. 841–844, Jun. 2019.

[159] T. Li, Y. Onodera, Y. Nakayama, and D. Hisano, "Multi-channel authentication for secure D2D using optical camera communication," in *Proc. IEEE 19th Annu. Consum. Commun. Netw. Conf.*, 2022, pp. 858–863.

[160] M. Plattner, E. Sonnleitner, and G. Ostermayer, "A security protocol for vehicle platoon verification using optical camera communications," *IEEE Trans. Intell. Transp. Syst.*, early access, Apr. 29, 2024, doi: 10.1109/TITS.2024.3390393.

[161] Y.-C. Chuang et al., "Using logistic regression classification for mitigating high noise-ratio advisement light-panel in rolling-shutter based visible light communications," *Opt. Exp.*, vol. 27, no. 21, pp. 29924–29929, Oct. 2019.

[162] J.-K. Lain, F.-C. Jhan, and Z.-D. Yang, "Non-line-of-sight optical camera communication in a heterogeneous reflective background," *IEEE Photon. J.*, vol. 11, no. 1, Feb. 2019, Art. no. 7900908.

[163] W. Guan, L. Huang, B. Hussain, and C. P. Yue, "Robust robotic localization using visible light positioning and inertial fusion," *IEEE Sens. J.*, vol. 22, no. 6, pp. 4882–4892, Mar. 2022.